Supporting Information

Snapshots of key intermediates unveiling the growth from silver ions to Ag_{70} nanoclusters

Xi-Ming Luo,[a] Shuo Huang,[a] Peng Luo,[b] Kai Ma,[a] Zhao-Yang Wang,[a] Xi-Yan Dong, [a, b] and Shuang-Quan Zang *[a]

[a]*Henan Key Laboratory of Crystalline Molecular Functional Materials, Henan International Joint Laboratory of Tumor Theranostical Cluster Materials, Green Catalysis Center, and College of Chemistry, Zhengzhou University, Zhengzhou 450001, China.*

[b]*College of Chemistry and Chemical Engineering, Henan Polytechnic University, Jiaozuo 454003, China*

Table of Contents

Experimental Procedures

Section S1. Materials and Methods

1.1 Materials and reagents.

The raw materials were purchased from Aladdin and used without further purification. All syntheses were carried out in 15 mL Teflon-lined reaction vessel under autogenous pressure.

1.2 X-ray crystallography.

SCXRD measurements were performed using a Rigaku XtaLAB Pro diffractometer with Cu-Kα radiation (λ = 1.54184 Å) for $\mathbf{Ag_{14}}$ and $\mathbf{Ag_{24}}$-$\mathbf{C_2F_5}$, as well as Mo-Kα radiation (λ = 0.71073 Å) for $\mathbf{Ag_{24}}$. Data collection and reduction were performed using *CrysAlis*^{Pro}. The structures were solved using intrinsic phasing methods (SHELXT-2015)[1] and refined by full-matrix least squares on F^2 using OLEX2,[2] which utilizes the SHELXL-2018/3 module.[3]

All hydrogen atoms were placed in their calculated positions with idealized geometries, and they possessed fixed isotropic displacement parameters. Appropriate restraints and/or constraints were applied to the geometry, and the atomic displacement parameters of the atoms in the cluster were determined. All non-H atoms were located in the electron density and refined with anisotropic thermal parameters. Due to disorder of the CF_3COO^-, FLAT restraints were applied to keep the planarity of F atoms; SADI and DFIX were applied to keep the distances of C–F (*ca.* 1.45 Å), C–C (*ca.*1.53 Å) and F···F of the CF_3COO^- in reasonable range; SAME restraints were applied to keep similar configurations of CF_3COO^- ligands. Besides, DFIX restraints were applied to keep the distances of C=O (*ca.* 1.2 Å), and C–N (*ca.*1.45 Å) of the DMF molecules in a reasonable range. ISOR, DELU and SIMU restraints were used for some atoms, especially peripheral F atoms with large thermal motion. All structures were examined using the Addsym subroutine of PLATON to ensure that no additional symmetry could be applied to the models.[4] A solvent mask has been used due to severe disorder of free solvent and $[NH_2(CH_3)_2]^+$ molecules around the cluster and diffract weakly.

Detailed information with respect to the X-ray crystal data, intensity collection procedure, and refinement results for the entire cluster compounds are summarized in Tables S1−S3.

1.3 Characterization.

UV–Vis absorption spectra (liquid) were recorded on a U-2000 spectrophotometer.

ESI-MS spectra were obtained on a SCIEX X500R QTOF LC/MS spectrometer.

1.4 Density functional theory (DFT) and time dependent density functional theory (TD-DFT) calculation.

Density functional theory (DFT) and time-dependent density functional theory (TD-DFT) calculations were performed using Gaussian 16[5] software with Perdew−Burke−Ernzerhof (PBE) functional.[6] All calculations were conducted using the Def2SVP basis set for H, C, O, N, F, S and Ag atoms.[7] The single crystal structure was chosen as an initial guess for ground-state optimization, and all reported stationary points were verified as true minima by the absence of negative eigenvalues in the vibrational frequency analysis. The calculated absorption spectra were obtained using Multiwfn 3.7 (dev).[8]

Section S2. Synthesis

Synthesis of Ag_{24} ($Ag_{24}S(S^iPr)_8(CF_3COO)_{10}(DMF)_8 \cdot 2(NH_2(CH_3)_2CF_3COO)$)

$\{Ag(S^iPr)\}_n$ (0.05 mmol, 9 mg) and CF_3COOAg (0.10 mmol, 22.1 mg) were dissolved together in a mixed solvent of ^{i}PrOH and DMF (4.0 mL, *v*:*v* = 3:1), and then, 50 μL of CF_3COOH was added to the above solution. The mixture was sealed in a 15-mL Teflon-lined reaction vessel and kept at 80°C for 3 h. After cooling to room temperature, the yellow solution was filtered and evaporated in the dark for 1 week. Yellow block crystals of **Ag_{24}** were isolated and washed with dichloride/n-hexane at a yield of 20% (based on $\{Ag(S^iPr)\}_n$). Elemental analysis (found (calcd), %; based on $C_{68}H_{112}Ag_{24}F_{30}N_8O_{28}S_9$): C, 17.46 (17.37); H, 2.39 (2.45); N, 2.72 (2.66); S, 5.31 (5.49).

Synthesis of Ag_{24}-C_2F_5 ($Ag_{24}S(S^iPr)_8(C_2F_5COO)_{10}(DMF)_8 \cdot 2(NH_2(CH_3)_2CF_3COO)$)

$\{Ag(S^iPr)\}_n$ (0.05 mmol, 9 mg) and C_2F_5COOAg (0.10 mmol, 27 mg) were dissolved together in a mixed solvent of ^{i}PrOH and DMF (4.0 mL, *v*:*v* = 3:1), and then, 50 μL of C_2F_5COOH was added to the above solution. The mixture was sealed in a 15-mL Teflon-lined reaction vessel and kept at 80°C for 3 h. After cooling to room temperature, the yellow solution was filtered and evaporated in the dark for 1 week. Yellow block crystals of **Ag_{24}-C_2F_5** were isolated and washed with dichloride/n-hexane at a yield of 25% (based on $\{Ag(S^iPr)\}_n$). Elemental analysis (found (calcd), %; based on $C_{79}H_{107}Ag_{24}F_{60}N_7O_{29}S_9$): C, 17.86 (18.05); H, 1.92 (2.20); N, 2.26 (2.39); S, 4.75 (4.93).

2.1. Different reaction time

$\{Ag(S^iPr)\}_n$ (0.05 mmol, 9 mg) and CF_3COOAg (0.10 mmol, 22.1 mg) were dissolved together in a mixed solvent of ^{i}PrOH and DMF (4.0 mL, *v*:*v* = 3:1), and then, 50 μL of CF_3COOH was added to the above solution. The mixture was sealed in a 15-mL Teflon-lined reaction vessel and kept at 80°C for 0−36 h (**0, 1, 2, 3, 4, 5, 6, 8, 10, 12, 15, 18, 24, and 36 h**). After cooling to room temperature, the solution was filtered and evaporated in the dark. Different crystals were obtained by evaporating the mother liquor from different reaction times at room temperature: 0 h, colorless block crystals (**Ag_{14}**); 3−6 h, yellow block crystals (**Ag_{24}**); 8−24 h, black octahedral crystals (**$Ag_{70} \cdot Ag_{12}$**); 36 h, black rectangular crystals (**Ag_{70}**).

The acquisition of **$Ag_{70} \cdot Ag_{12}$** as a transition product shows that when the number of Ag_{70} was relatively small, the Ag_{70} nanoclusters tend to co-crystallize with small Ag species. With most of the silver species transformed into Ag_{70}, the nanoclusters will crystallize by themselves and precipitate out.

2.2. Different amounts of DMF

$\{Ag(S^iPr)\}_n$ (0.05 mmol, 9 mg) and CF_3COOAg (0.10 mmol, 22.1 mg) were dissolved together in a mixed solvent of (4-x) mL ^{i}PrOH and x mL DMF (**x = 0, 0.2, 0.4, 0.6, 0.8, 1.0, 1.2, 1.4, 1.6, 1.8, 2.0, 3.0, and 4.0**), and then, 50 μL of CF_3COOH was added to the above solution. The mixture was sealed in a 15-mL Teflon-lined reaction vessel and kept at 80°C for 24 h. After cooling to room temperature, the solution was filtered and evaporated in the dark. After several days of evaporation of mother liquor from different reaction conditions at room temperature, different crystals were obtained: 1.0 mL DMF (3.0 mL ^{i}PrOH) and 1.2 mL DMF (2.8 mL ^{i}PrOH), black octahedral crystals (**$Ag_{70} \cdot Ag_{12}$**); 1.4 mL DMF (2.6 mL ^{i}PrOH), black octahedral crystals (**$Ag_{70} \cdot Ag_{12}$**) and black rectangular crystals (**Ag_{70}**); 1.6 mL DMF (2.4 mL ^{i}PrOH), black rectangular crystals (**Ag_{70}**); others, no crystals.

2.3. Different amounts of CF_3COOH

$\{Ag(S^iPr)\}_n$ (0.05 mmol, 9 mg) and CF_3COOAg (0.10 mmol, 22.1 mg) were dissolved together in a mixed solvent of 3 mL ^{i}PrOH and 1 mL DMF, and then, a certain amount of CF_3COOH (**0, 10, 20, 30, 40, 50, 60, 70, 80, 90, 100, 125, 150, 175, 200, 250 μL**) was added to the above solution. The mixture was sealed in a 15-mL Teflon-lined reaction vessel and kept at 80°C for 24 h. After cooling to room temperature, the solution was filtered and evaporated in the dark. After several days of evaporation of mother liquor from different reaction conditions at room temperature, different crystals were obtained: 40, 50, and 60 μL CF_3COOH, black octahedral crystals (**$Ag_{70} \cdot Ag_{12}$**); 70 μL CF_3COOH, black octahedral crystals (**$Ag_{70} \cdot Ag_{12}$**) and black rectangular crystals (**Ag_{70}**); 80, 90, and 100 μL CF_3COOH, black rectangular crystals (**Ag_{70}**); others, no crystals.

Results and Discussion

Section S3. Supplementary Figures

3.1 Tracking the reaction process based on the colour and UV-Vis of mother liquor

A series of improved experiments (Figs. S1−S4) were used to achieve our goal: $\{Ag(S^iPr)\}_n$ (0.05 mmol, 9 mg) and CF_3COOAg (0.10 mmol, 22 mg) together with CF_3COOH (0−250 μL) were mixed and reacted in the 4 mL organic solvent containing DMF and ^{i}PrOH, under solvothermal conditions at 80 ℃ (1−36 h).

Through different reaction time (1−36 h) to control the reduction process (CF_3COOH: 50 μL; DMF: 1 mL; ^{i}PrOH: 3 mL), the color of the mother liquor is significantly different (Fig. 1). From colorless (0−1 h) to yellow (2−3 h), then to orange (4−6 h), red (8−10 h), and finally to black red (over 12 h), this indicates that the reduction degree of the system gradually deepened. Time-dependent UV-Vis absorption spectra (Fig. 1b and Fig. S1) show the characteristic peak (*ca.* 530 nm) of **Ag$_{70}$** appeared after 4 hours (Fig. S1d), corresponding to the change of mother liquor from yellow to orange (Fig. 1). After reaction for 24 hours, UV-Vis spectra of mother liquor were basically consistent with that of **Ag$_{70}$** (Fig. S1c). Interestingly, when the mother liquor was yellow (reaction time: 2−3 h), only a characteristic absorption sharp peak (416 nm) that did not belong to the **Ag$_{70}$** appeared in the UV-Vis spectrum (Fig. S1d), suggesting that intermediate substances may have been formed during the formation of **Ag$_{70}$**. The product of the reaction for 3 hours was filtered and evaporated at room temperature to obtain yellow crystals (Fig. 2c), $S@Ag_{24}(S^iPr)_8(CF_3COO)_{10}(DMF)_{10}$, **Ag$_{24}$** in short. The characteristic absorption peak (*ca.* 420 nm) of **Ag$_{24}$** corresponds well with mother liquor (reaction time: 3 h), indicating that the main substance in the mother liquor at this time is **Ag$_{24}$** clusters. With the continuous generation of **Ag$_{24}$** in the mother liquor, multiple **Ag$_{24}$** clusters with high reactive activity generate more stable **Ag$_{70}$** through collision, self-assembly and fusion, so the characteristic peak (*ca.* 530 nm) of **Ag$_{70}$** gradually appears and rapidly increases (Fig. S1a−b).

Parallel experiments (variable: DMF (Figs. S2−S3) or CF_3COOH (Fig. S4)) also have similar phenomena, which suggest intermediate substances. The appropriate amount (*ca.* 1.0−1.6 mL) of DMF can effectively prepare **Ag$_{70}$** clusters (Fig.S2). **Ag$_{70}$** cannot be generated effectively if the DMF content in the mixed solution is too low (*ca.* 0.2−0.8 mL, Fig. S2) or too high (*ca.* 1.8−4.0 mL, Figs. S2−S3). As shown in Fig. S2b, when DMF content is low (*ca.* 0.2−0.8 mL), the characteristic peak of **Ag$_{24}$** is obvious, while **Ag$_{70}$** is weak. It may be caused by the poor efficiency of conversion from **Ag$_{24}$** to **Ag$_{70}$**. As shown in Fig. S2c and Fig. S3, when DMF content is large (*ca.* 1.8−4.0 mL), no characteristic peak was observed, possibly caused by the inability to form **Ag$_{24}$** (*ca.* 1.8−4.0 mL).

The introduction of CF_3COOH may be a necessary factor in the formation of **Ag$_{24}$** (Fig. S4). As shown in Fig. S4b, **Ag$_{24}$** cannot be formed without or with only a small amount (10 μL) of CF_3COOH. Meanwhile, excess acid (> 100 μL) also inhibits the formation of the products (Fig. S4c). Increasing the amount of $\{Ag(S^iPr)\}_n$ (0.05 mmol→0.10 mmol) in the reactants had little effect on the final result (Fig. S5).

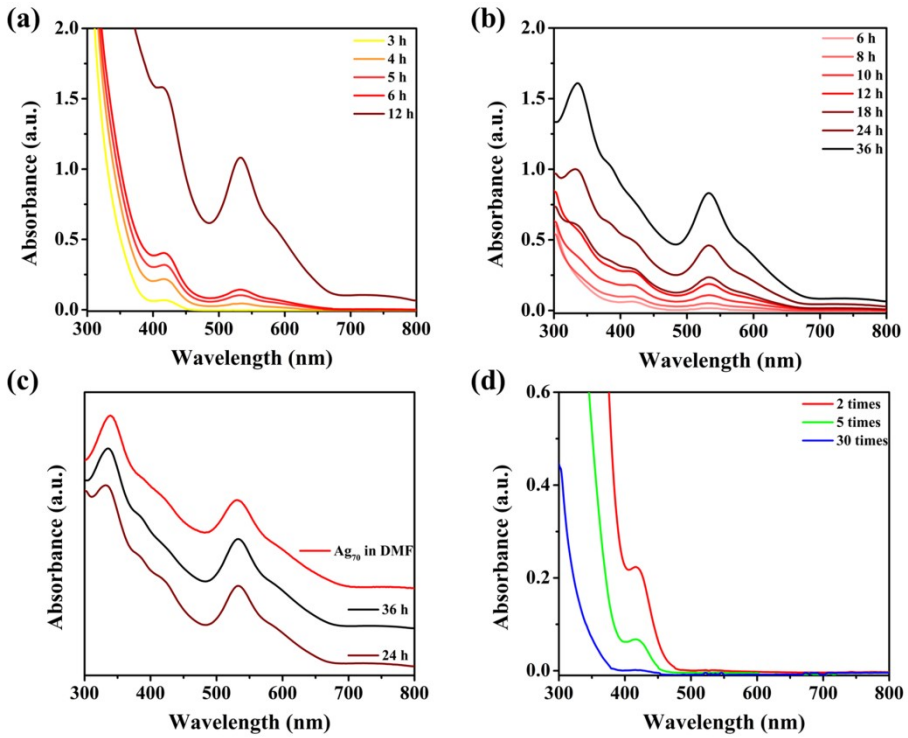

Fig. S1 (a) UV-Vis absorption spectra of mother liquor after solvothermal reaction at different times of 3, 4, 5, 6, and 12 hours (diluted 5 times by DMF). (b) UV-Vis absorption spectra of mother liquor after solvothermal reaction at different times of 6, 8, 10, 12, 18, 24, and 36 hours (diluted 30 times by DMF). (c) Comparing the UV-Vis absorption spectra of **Ag_{70}**, 24 h and 36 h mother liquor. (d) UV-Vis absorption spectra of mother liquor after 3 h solvothermal reaction (diluted 2, 5, and 30 times by DMF).

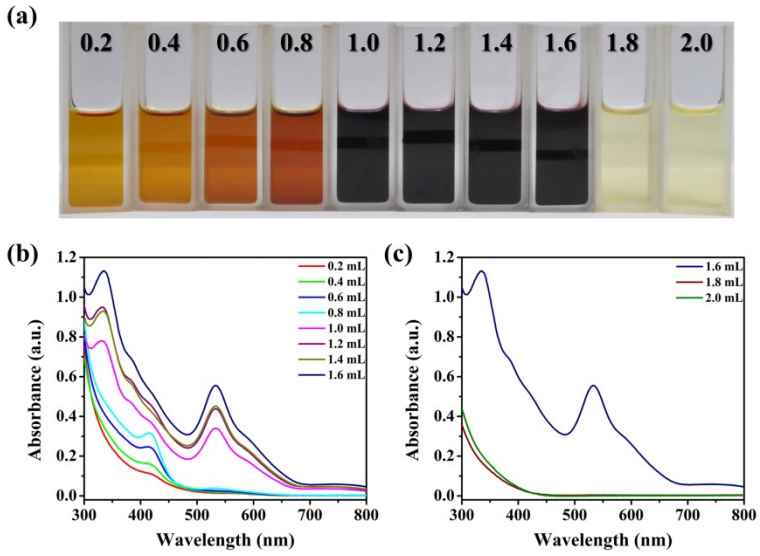

Fig. S2 (a) The color of mother liquor after solvothermal reaction at different mixture solvents (v(DMF) + v(^{i}PrOH) = 4 mL): the volume of DMF is 0.2, 0.4, 0.6, 0.8, 1.0, 1.2, 1.4, 1.6, 1.8, and 2.0 mL, respectively (from left to right). (b−c) Time-dependent UV-Vis absorption spectra for tracking the reaction process (diluted 30 times by DMF). Specific methods are as follows: transfer 100 μL of mother liquor to a quartz cuvette, and then put 2.9 mL DMF to dilute the sample.

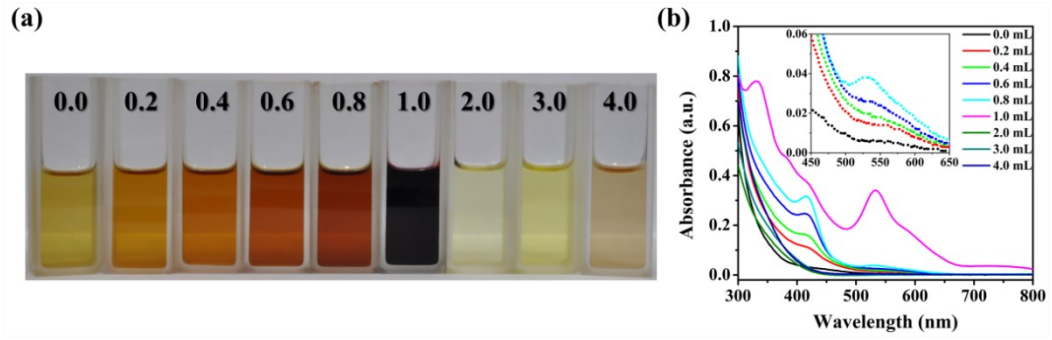

Fig. S3 (a) The color of mother liquor after solvothermal reaction at different mixture solvents (v(DMF) + v(^{i}PrOH) = 4 mL): the volume of DMF is 0.0, 0.2, 0.4, 0.6, 0.8, 1.0, 2.0, 3.0, and 4.0 mL, respectively (from left to right). (b) Time-dependent UV-Vis absorption spectra for tracking the 3a reaction process (diluted 30 times by DMF).

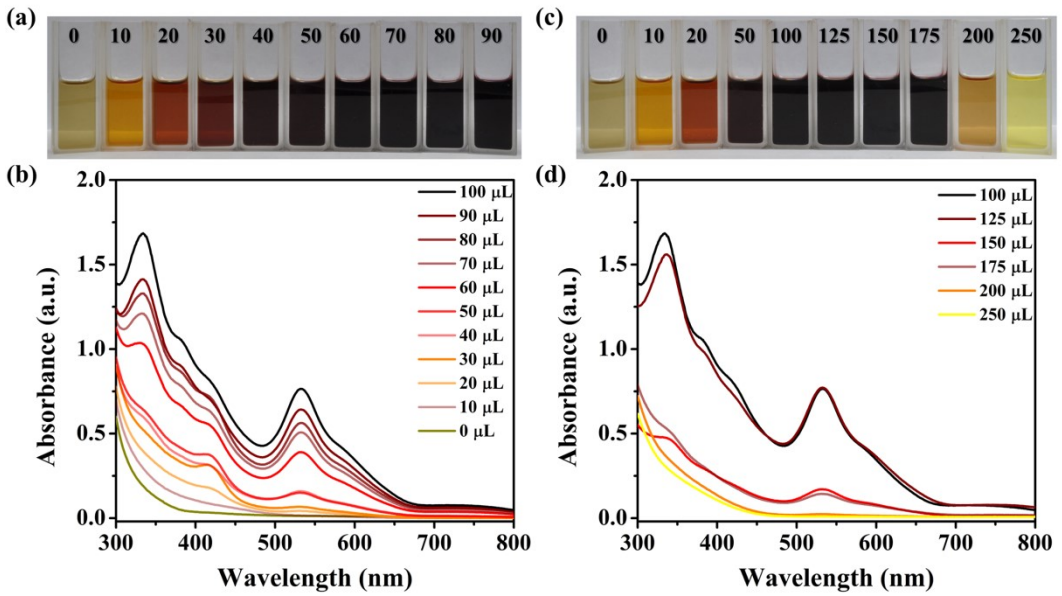

Fig. S4 (a) The color of mother liquor after solvothermal reaction at different CF_3COOH. From left to right, the volume of CFCOOH is 0, 10, 20, 30, 40, 50, 60, 70, 80 and 90 µL, respectively. (b) Time-dependent UV-Vis absorption spectra for tracking the 4a reaction process (diluted 30 times by DMF). (c) The color of mother liquor after solvothermal reaction at different CF_3COOH. From left to right, the volume of CFCOOH is 0, 10, 20, 50, 100, 125, 150, 175, 200 and 250 µL, respectively. (d) Time-dependent UV-Vis absorption spectra for tracking the 4c reaction process (diluted 30 times by DMF).

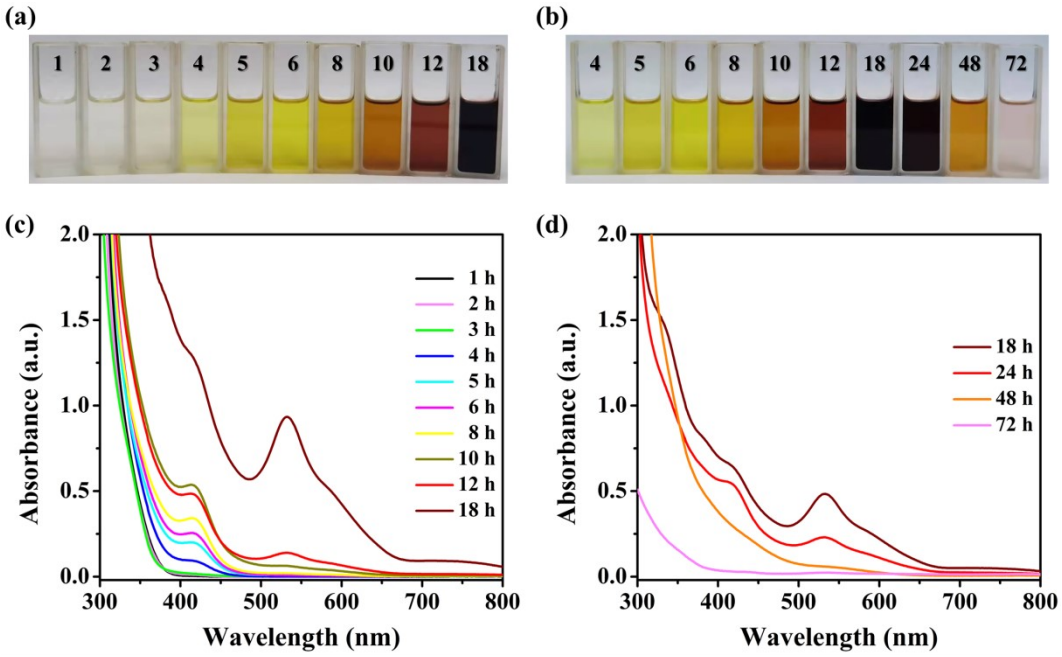

Fig. S5 (a, b) The color of mother liquor after solvothermal reaction (13.5 mg $\{Ag(S^iPr)\}_n$, 22 mg CF_3COOAg, and 50 μL CF_3COOH in mixture solvent (^{i}PrOH : DMF = 3 : 1) at 80 ℃) for different times (1, 2, 3, 4, 5, 6, 8, 10, 12, 18, 24, 48, and 72 hours); (c, d) UV-Vis absorption spectra (diluted 10 times by DMF). Among them, mother liquor (18 and 24 h) in (d) was diluted 20 times for comparison.

3.2 Tracking the reaction process based on ESI-MS of mother liquor

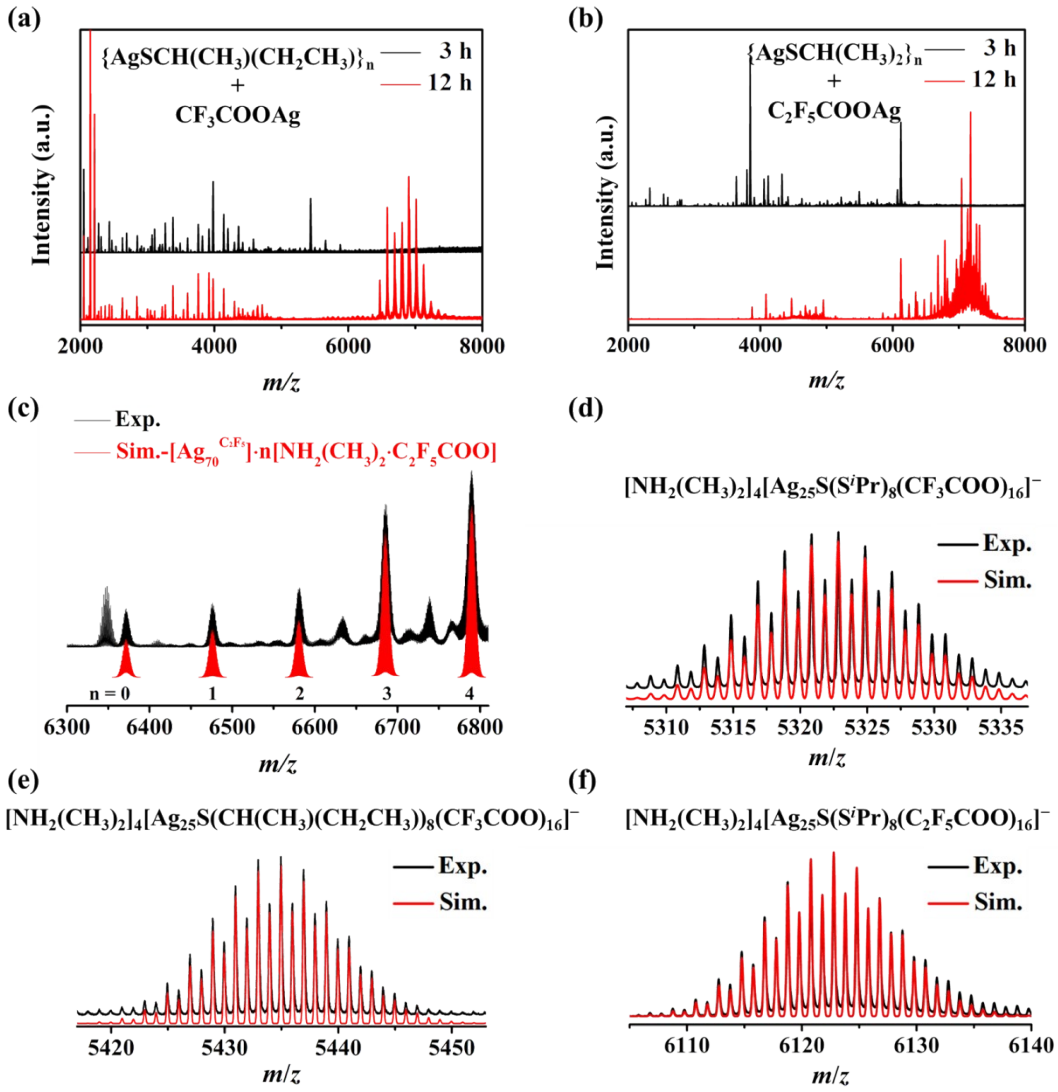

Fig. S6 (a) Negative ion mode ESI-MS in range of m/z = 2000−8000 on the reaction of 10 mg $\{Ag(SCH(CH_3)(CH_2CH_3))\}_n$, 22 mg CF_3COOAg, and 50 μL CF_3COOH in mixture solvent (^{i}PrOH : DMF = 3 : 1) at 3 and 12 hours at 80 °C. (b) Negative ion mode ESI-MS in range of m/z = 2000−8000 on the reaction of 10 mg $\{Ag(SCH(CH_3)_2)\}_n$, 30 mg C_2F_5COOAg, and 70 μL C_2F_5COOH in mixture solvent (^{i}PrOH : DMF = 3 : 1) at 3 and 24 hours at 80 °C. (c) Experimental (Exp.) in 24 h (b) and simulated (Sim.) mass spectra (m/z = 6300−6810) of the isotopic envelopes; (d−f) Experimental (Exp.) and simulated (Sim.) mass spectra of the isotopic envelopes for $\{[NH_2(CH_3)_2]_4[Ag_{25}S(SCH(CH_3)_2)_8(CF_3COO)_{16}]\}^-$, 4e (d); $\{[NH_2(CH_3)_2]_4[Ag_{25}S(SCH(CH_3)(CH_2CH_3))_8(CF_3COO)_{16}]\}^-$, 4e (e); $\{[NH_2(CH_3)_2]_4[Ag_{25}S(SCH(CH_3)_2)_8(C_2F_5COO)_{16}]\}^-$, 4e (f).

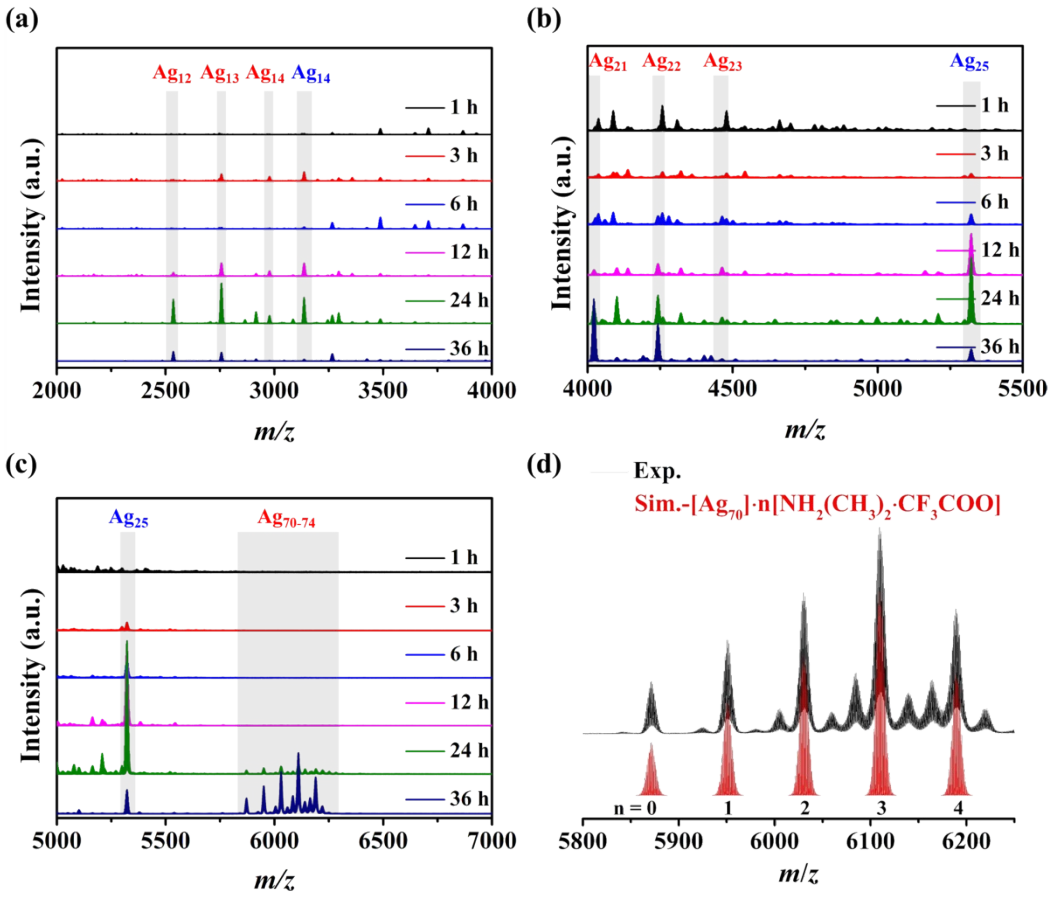

Fig. S7 Time-dependent negative ion mode ESI-MS in range of *m*/*z* = 2000−7000 on the reaction of 9 mg $\{Ag(S^iPr)\}_n$, 22 mg CF_3COOAg, and 50 μL CF_3COOH in mixture solvent (^{i}PrOH : DMF = 3 : 1) at 1, 3, 6, 12, 24, and 36 hours at 80 °C: (a) *m*/*z* = 2000−4000. (b) *m*/*z* = 4000−5500. (c) *m*/*z* = 5000−7000. (d) Experimental (Exp.) in 36 h and simulated (Sim.) mass spectra (*m*/*z* = 5800−6250) of the isotopic envelopes.

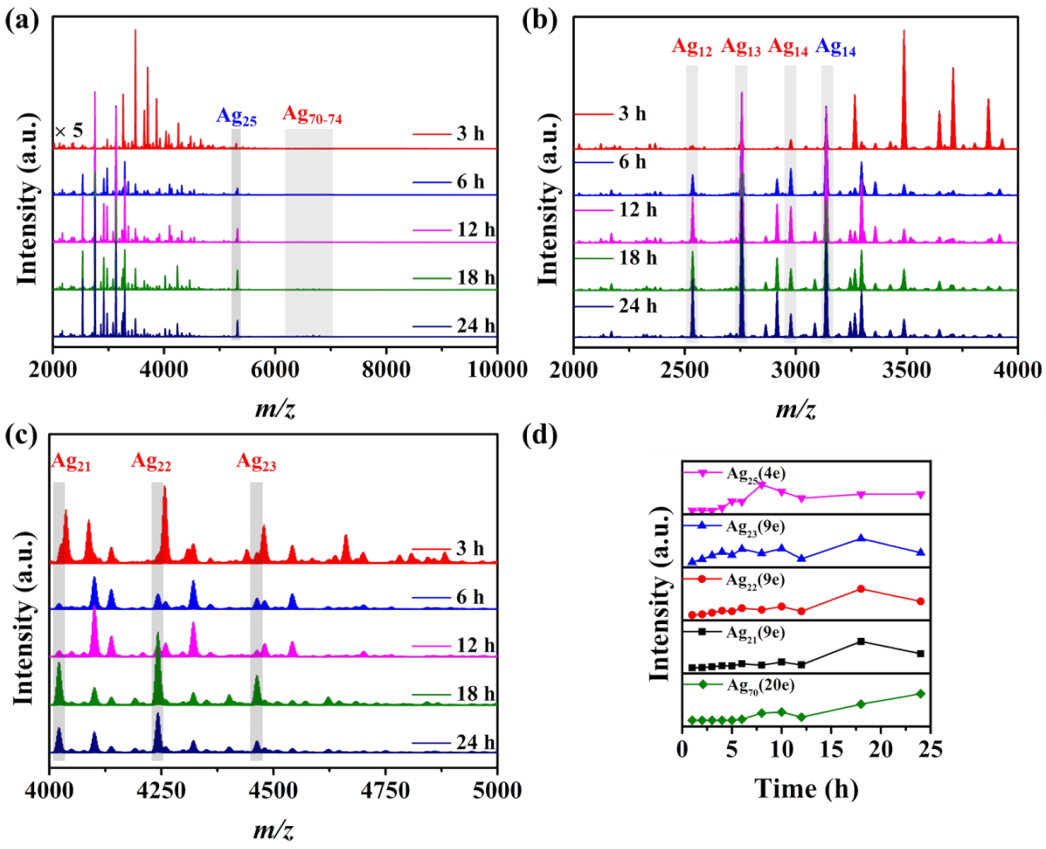

Fig. S8 Time-dependent negative ion mode ESI-MS in range of *m*/*z* = 2000−10000 on the reaction of 13.5 mg $\{Ag(S^iPr)\}_n$, 22 mg CF_3COOAg, and 50 μL CF_3COOH in mixture solvent (^{i}PrOH : DMF = 3 : 1) at 3, 6, 12, 18, and 24 hours at 80 °C: (a) *m*/*z* = 2000−10000. (b) *m*/*z* = 2000−4000. (c) *m*/*z* = 4000−5000. (d) Intensity-base profiles of $\{Ag_{25}\}$, $\{Ag_{23}\}$, $\{Ag_{22}\}$, $\{Ag_{21}\}$, and $\mathbf{Ag_{70}}$.

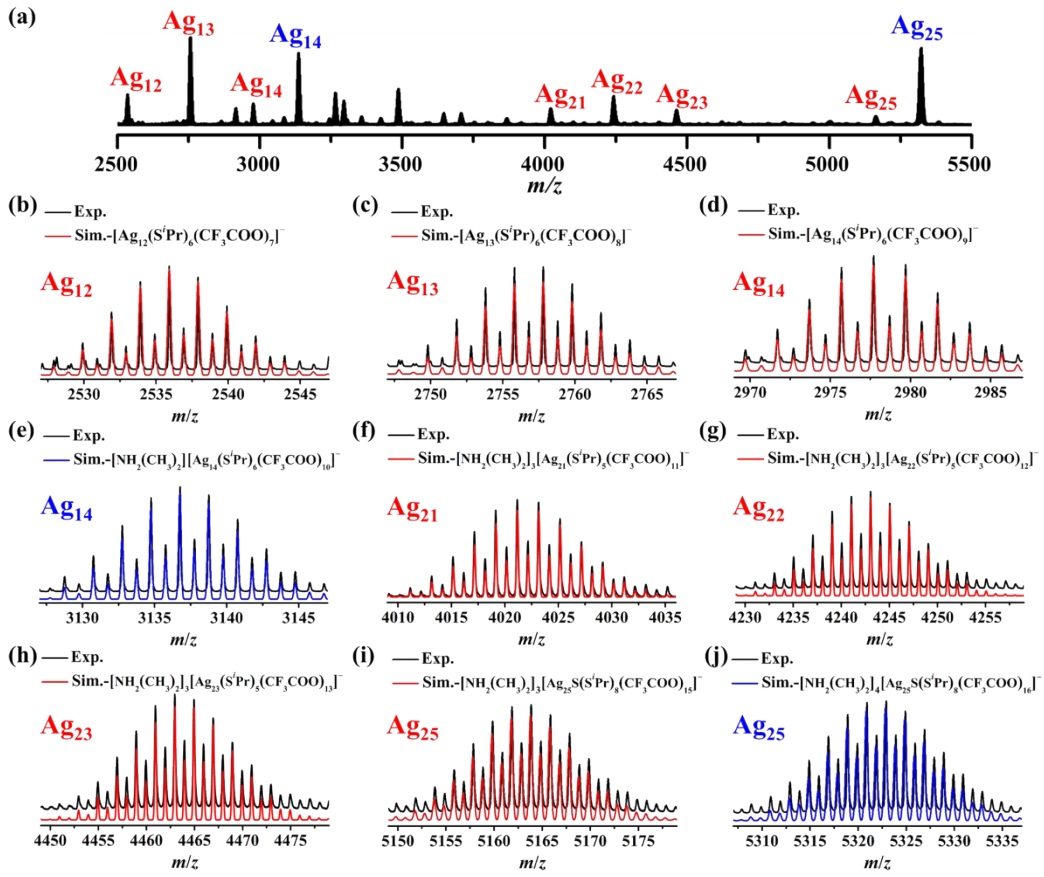

Fig. S9 (a) Negative ion mode ESI-MS (*m/z* = 2500−5500) on the reaction of 9.0 mg $\{Ag(S^iPr)\}_n$, 22 mg CF_3COOAg, and 50 μL CF_3COOH in mixture solvent (^{i}PrOH : DMF = 3 : 1) for 12h at 80 °C. (b–j) Experimental (Exp.) and simulated (Sim.) mass spectra of the isotopic envelopes for $[Ag_{12}(S^iPr)_6(CF_3COO)_7]^-$, 0e (b); $[Ag_{13}(S^iPr)_6(CF_3COO)_8]^-$, 0e (c); $[Ag_{14}(S^iPr)_6(CF_3COO)_9]^-$, 0e (d); $[NH_2(CH_3)_2][Ag_{14}(S^iPr)_6(CF_3COO)_{10}]^-$, 0e (e); $\{[NH_2(CH_3)_2]_3[Ag_{21}(S^iPr)_5(CF_3COO)_{11}]\}^-$, 9e (f); $\{[NH_2(CH_3)_2]_3[Ag_{22}(S^iPr)_5(CF_3COO)_{12}]\}^-$, 9e (g); $\{[NH_2(CH_3)_2]_3[Ag_{23}(S^iPr)_5(CF_3COO)_{13}]\}^-$, 9e (h); $\{[NH_2(CH_3)_2]_3[Ag_{25}S(S^iPr)_8(CF_3COO)_{15}]\}^-$, 4e (i); $\{[NH_2(CH_3)_2]_4[Ag_{25}S(S^iPr)_8(CF_3COO)_{16}]\}^-$, 4e (f).

3.3 Structure

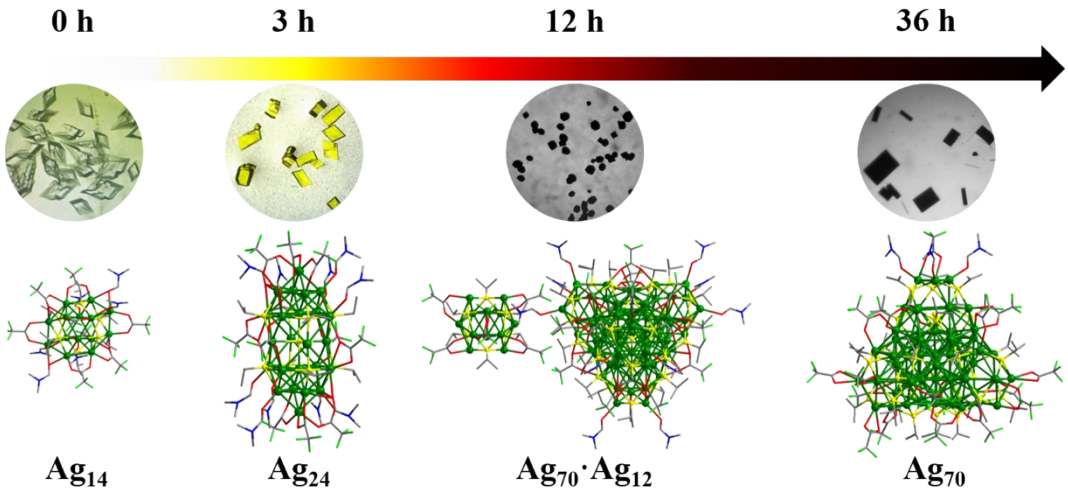

Fig. S10 The photographic images and structures of crystals precipitated from mother liquor under solvothermal reaction at different times: 0 h, colourless crystal, **Ag_{14}**; 3 h, yellow crystal, **Ag_{24}**; 12 h, black octahedral crystal, **Ag_{70}·Ag_{12}**; 36 h, black rectangular crystal, **Ag_{70}**.

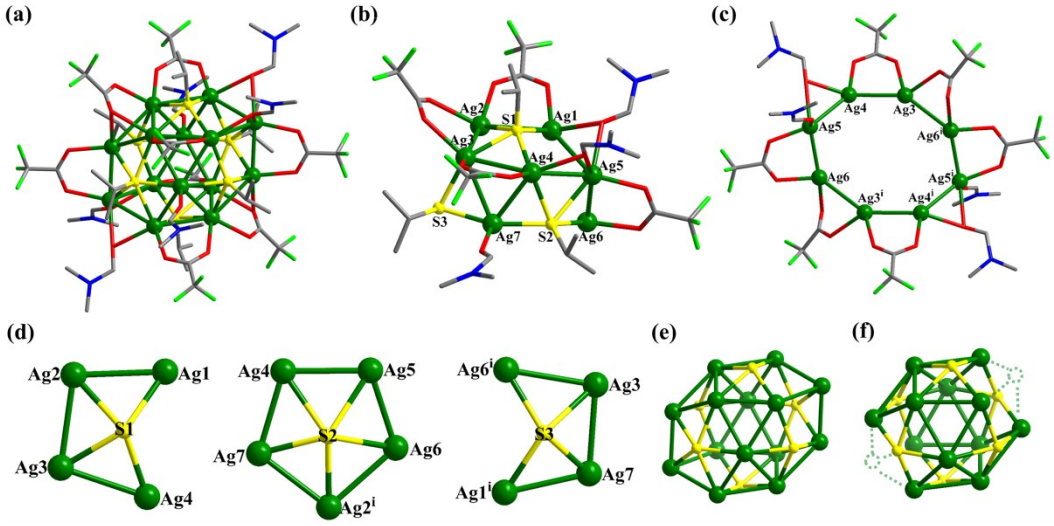

Fig. S11 The crystal structure of **Ag_{14}**. (a) The total structure. (b) The asymmetric unit. (c) The middle silver ring protected and stablized by CF_3COO^- and DMF. (d) The coordination modes of three crystallographically independent S atoms from different S^iPr^- ligands. (e) The Ag-S skeleton of **Ag_{14}**. (f) The Ag-S skeleton of the Ag_{12} of **Ag_{70}·Ag_{12}**. It can be considered that Ag_{14} is missing two horns (Ag ions). Atom color codes: green, Ag; yellow, S; red, O; bright green, F; blue, N; grey, C. All hydrogen atoms are omitted for clarity. Symmetry code: ^{i}1.5-x, 1.5-y, 1-z.

SCXRD result shows that **Ag_{14}** ($Ag_{14}(S^iPr)_6(CF_3COO)_8(DMF)_6$, Fig. S11a) crystallizes in monoclinic space group *C*2/*c* (No. 15) and half a cluster ($Ag_7(S^iPr)_3(CF_3COO)_4(DMF)_3$) exists in the asymmetric unit (Fig. S11b). **Ag_{14}** is a centrosymmetric ellipsoidal cluster and contains an $Ag_{14}S_6$ shell (Fig. S11e) protected by eight CF_3COO^- and six DMF molecules. Based on their coordination modes, six S^iPr^- ligands are divided into two types comprised of 4 μ_4 (Ag_4 trapezoids) and 2 μ_5 (Ag_5 pentagon) modes (Fig. S11d) with Ag−S bond lengths ranging from 2.462(4)−2.550(5) Å, 2.473(4)−2.682(5) Å, respectively. By sharing vertices with each other, the Ag_4 trapezoids and Ag_5 pentagons are linked together to form a hollow ellipsoidal $Ag_{14}S_6$ cage, which exhibits a three-layer Ag_3−Ag_8−Ag_3 (triangle-octagon-triangle) skeletal arrangement. The distances of Ag···Ag interactions range from 2.835(3) to 3.335(3) Å (Table S2), indicating that there are significant argentophilic interactions in consolidating the **Ag_{14}** cluster. The Ag_3 triangle at both ends is covered and stabilized by one CF_3COO^- ligand (coordination mode: μ_2-η^1,η^1) and one DMF molecule, while Ag_8 octagon ring in the middle is surrounded by six CF_3COO^- ligands (coordination modes: μ_2-η^1,η^1 and μ_3-η^1:η^2) and four DMF molecules on the outside. The Ag−O(CF_3COO^-) and Ag−O(DMF) bond lengths span from 2.24(3)−2.77(3) Å, 2.28(3)−2.51(2) Å, respectively.

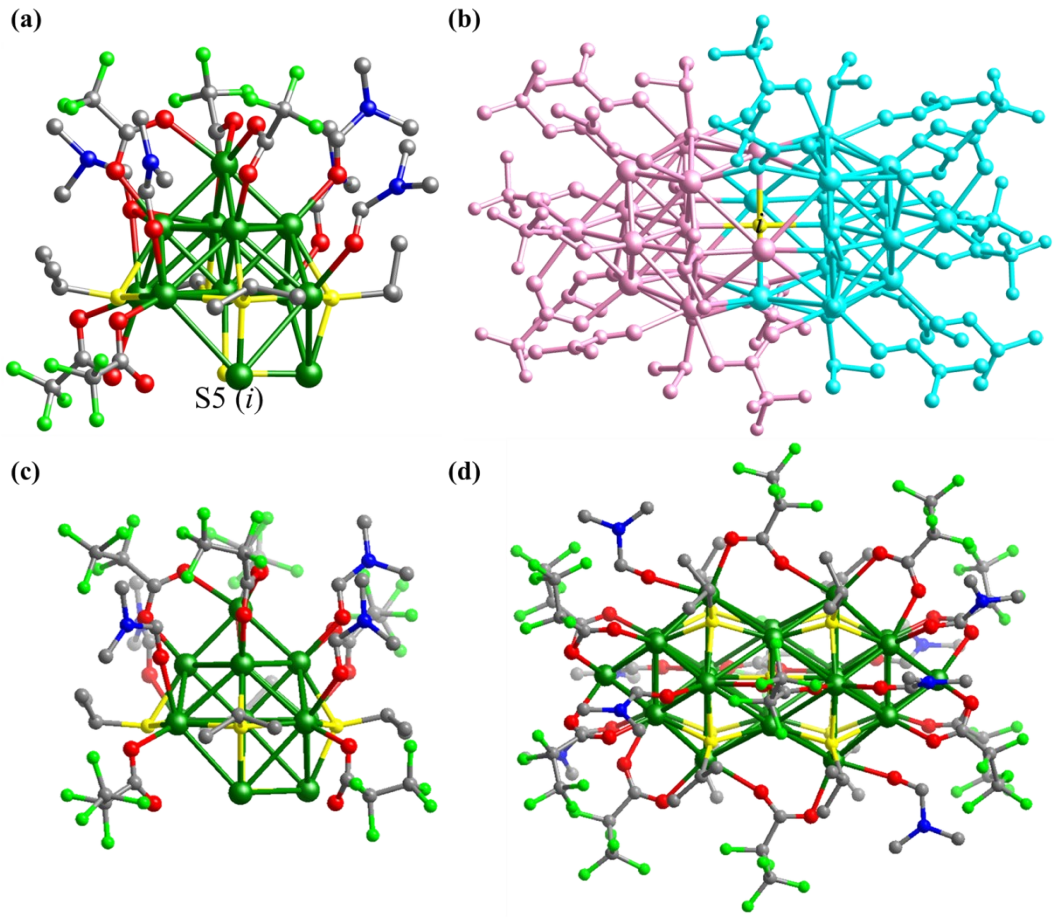

Fig. S12 The crystal structure of **Ag_{24}** and **Ag_{24}-C_2F_5**. (a) The asymmetric unit of **Ag_{24}**. (b) The total structure of **Ag_{24}**, containing two asymmetric units sharing a S atom (S5) at the inversion center (*i*). (c) The asymmetric unit of **Ag_{24}-C_2F_5**. (d) The total structure of **Ag_{24}-C_2F_5**.

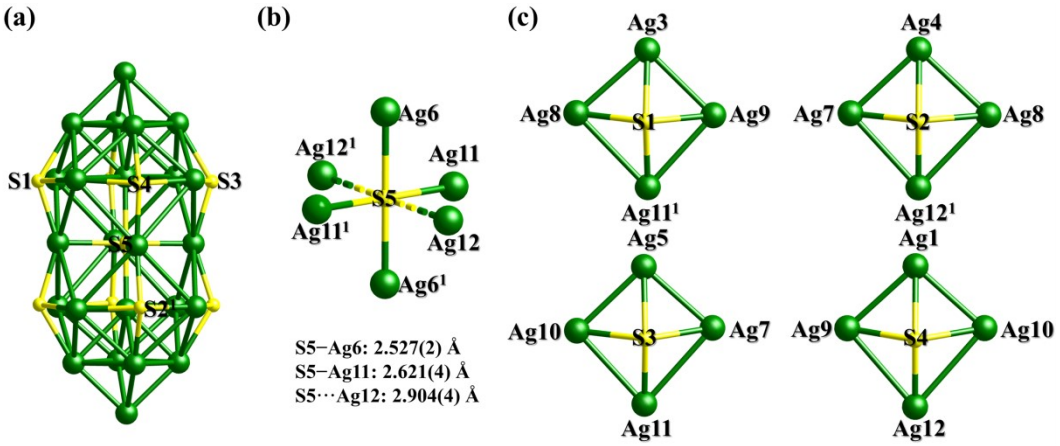

Fig. S13 The S@$Ag_{24}S_8$ framework of **Ag_{24}** and the coordination modes of five crystallographically independent S atoms (one from S^{2-}, others from S^iPr^- ligands).

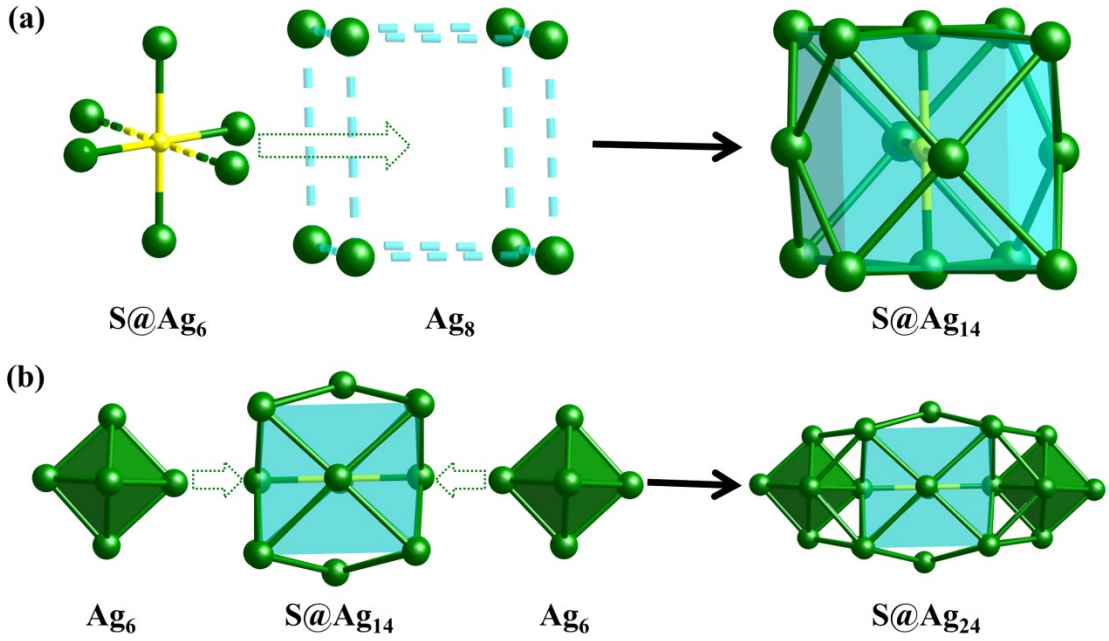

Fig. S14 The $S@Ag_{24}$ skeleton of **Ag_{24}**. (a) The S^{2-} acts as a template to induce a distorted octahedron $S@Ag_6$, which is confined within a slightly twisted cube Ag_8. $S@Ag_{14}$ ($S@Ag_6@Ag_8$) was viewed as the middle segment of the **Ag_{24}** cluster. (b) Fusion of $S@Ag_{14}$ and two Ag_6 cores into a $S@Ag_{24}$ kernel in the **Ag_{24}** nanocluster.

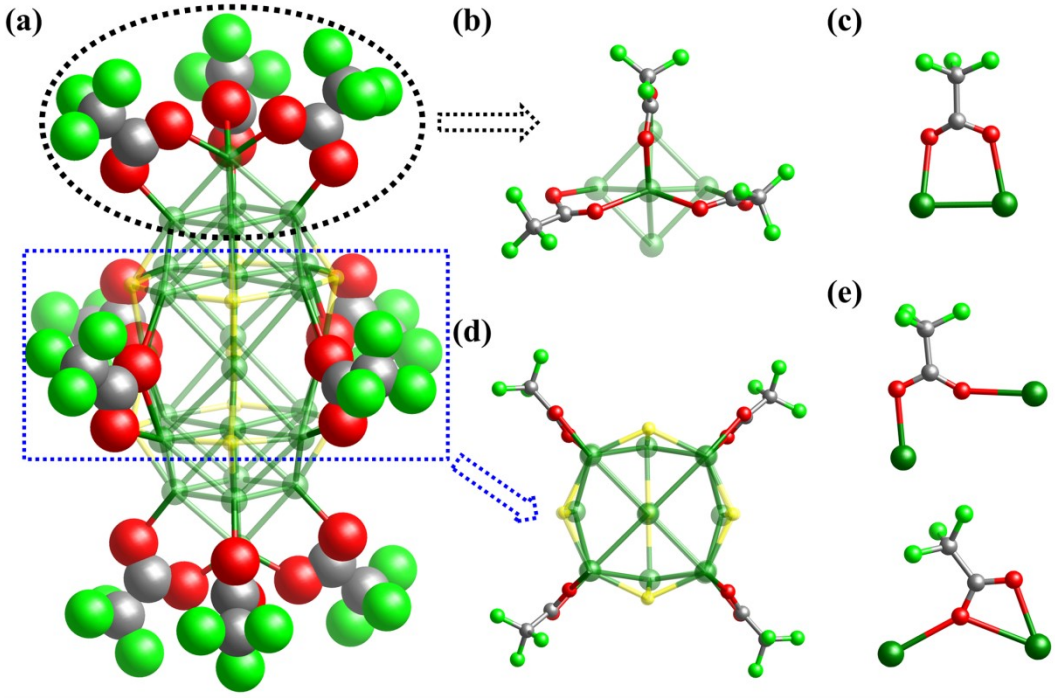

Fig. S15 The distribution and coordination modes of ten CF_3COO^- ligands on the surface of **Ag_{24}**.

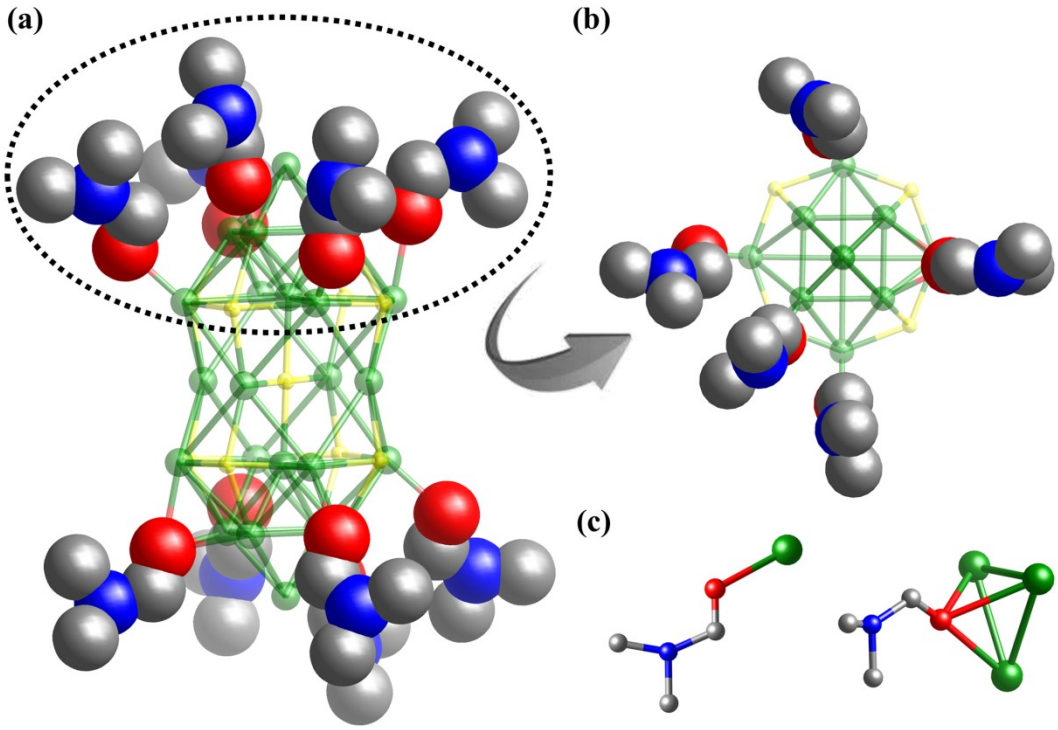

Fig. S16 The distribution and coordination modes (μ_1 and μ_3) of ten coordinated DMF molecules on the surface of $\mathbf{Ag_{24}}$.

3.4 Characterization of properties of Ag_{24}

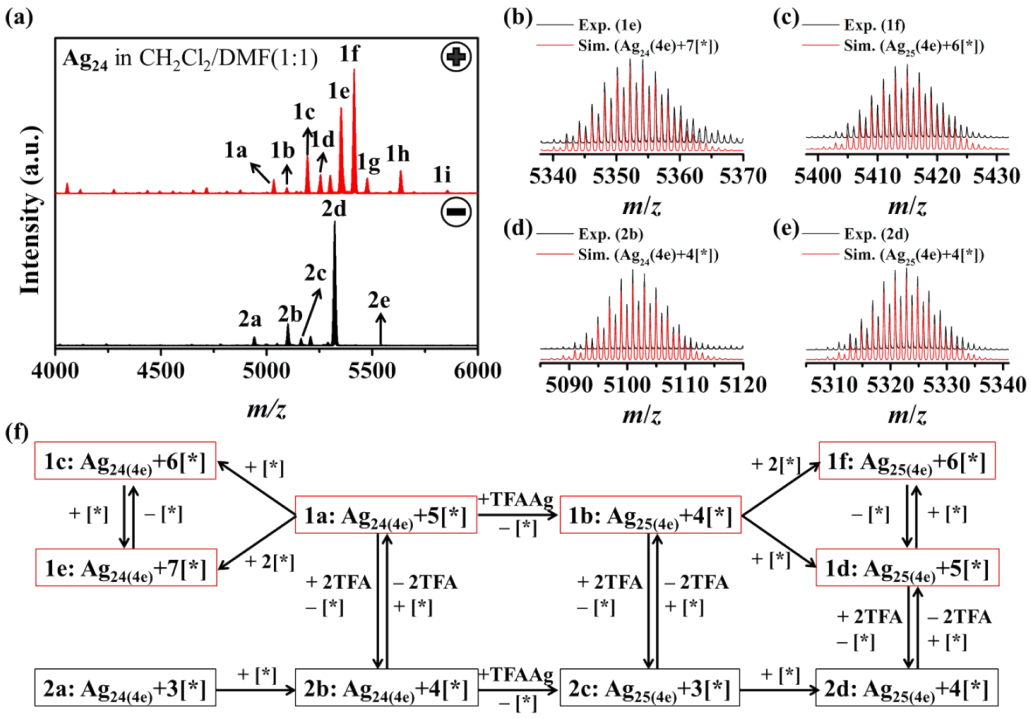

Fig. S17 (a) The position and negative ion mode ESI-MS (*m/z* = 4000−6000) of **Ag_{24}** in CH_2Cl_2/DMF (*v*:*v* = 1:1). (b−e) Experimental (Exp.) and simulated (Sim.) mass spectra of the main isotopic envelopes for $\{[NH_2(CH_3)_2]_7[Ag_{24}S(S^iPr)_8(CF_3COO)_{16}]\}^+$ (b); $\{[NH_2(CH_3)_2]_6[Ag_{25}S(S^iPr)_8(CF_3COO)_{16}]\}^+$ (c); $\{[NH_2(CH_3)_2]_4[Ag_{24}S(S^iPr)_8(CF_3COO)_{15}]\}^-$ (d); $\{[NH_2(CH_3)_2]_4[Ag_{25}S(S^iPr)_8(CF_3COO)_{16}]\}^-$ (e). (f) The correlations of the main envelopes of **1a**–**1f** and **2a**–**2d**. Note: [*] = $[NH_2(CH_3)_2][CF_3COO]$, $TFA^- = CF_3COO^-$.

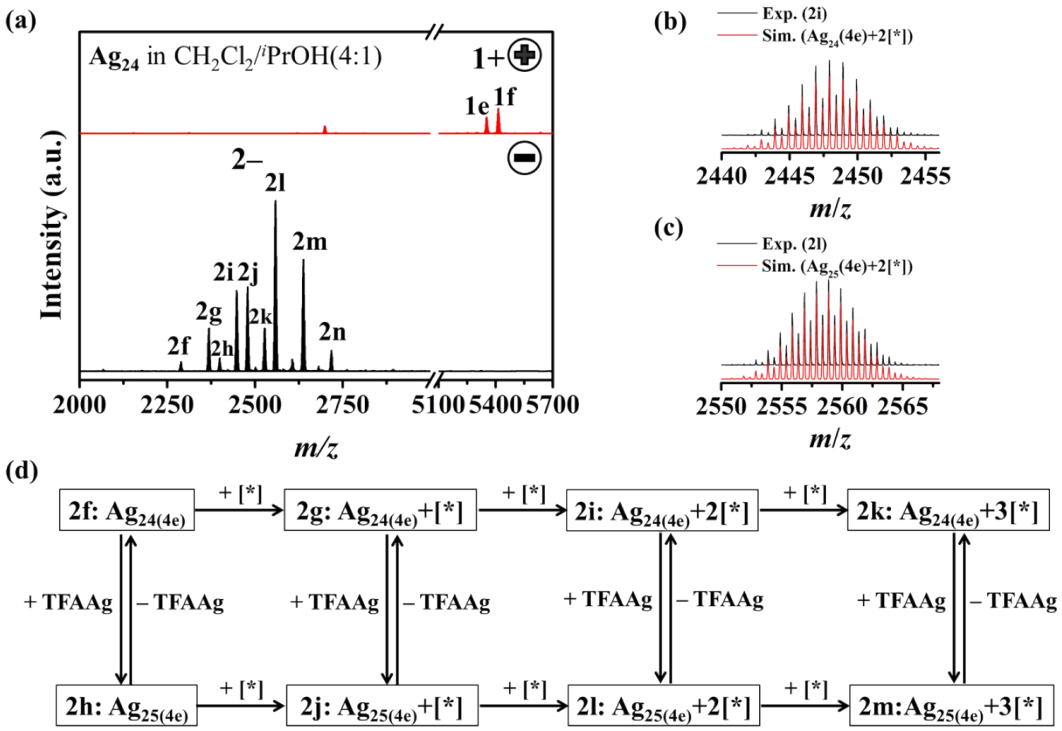

Fig. S18 (a) The position and negative ion mode ESI-MS (*m/z* = 2000−5700) of **Ag_{24}** in CH_2Cl_2/^{i}PrOH (*v*:*v* = 4:1). (b−c) Experimental (Exp.) and simulated (Sim.) mass spectra of the main isotopic envelopes for $\{[NH_2(CH_3)_2]_2[Ag_{24}S(S^iPr)_8(CF_3COO)_{14}]\}^{2-}$ (b); $\{[NH_2(CH_3)_2]_2[Ag_{25}S(S^iPr)_8(CF_3COO)_{15}]\}^{2-}$ (c). (d) The correlations of the main envelopes of **2f**–**2m**. Note: [*] = $[NH_2(CH_3)_2][CF_3COO]$, TFA^- = CF_3COO^-.

3.5 Theoretical calculation of Ag_{24}

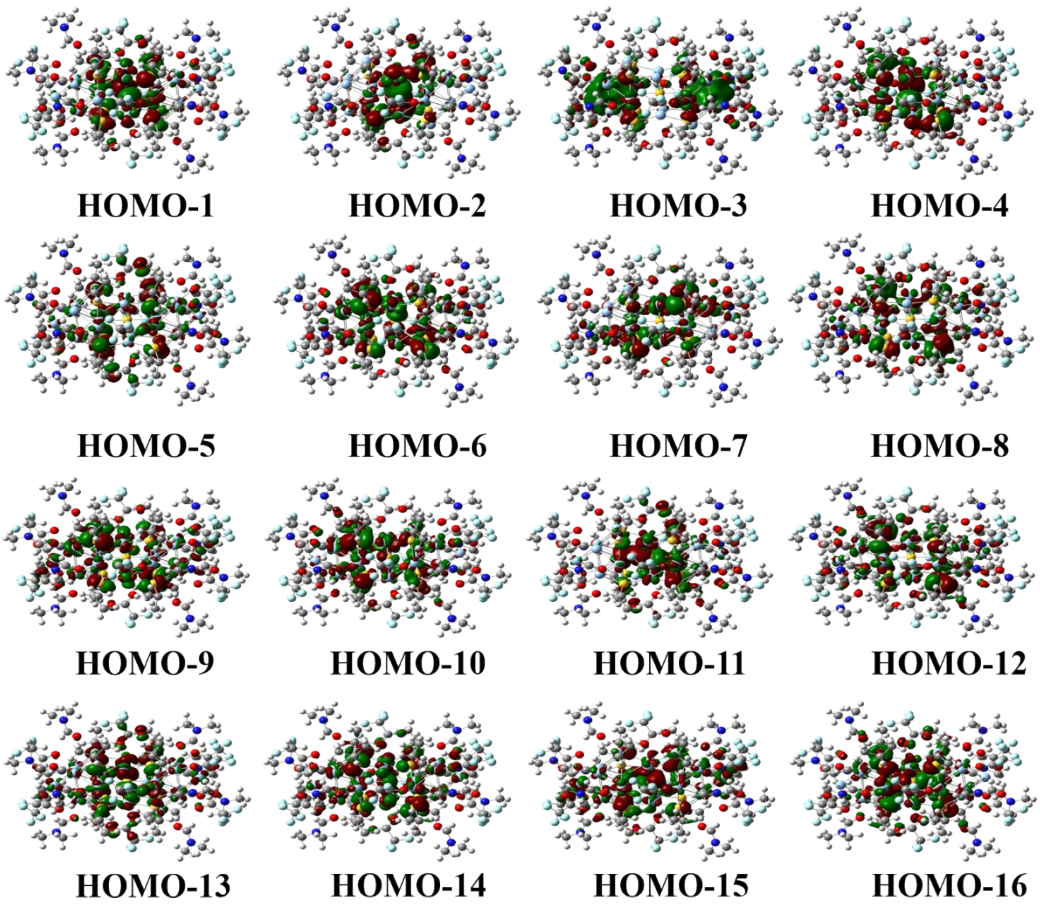

Fig. S19 Orbital diagrams involved in the α, β, and γ transitions of **Ag_{24}**.

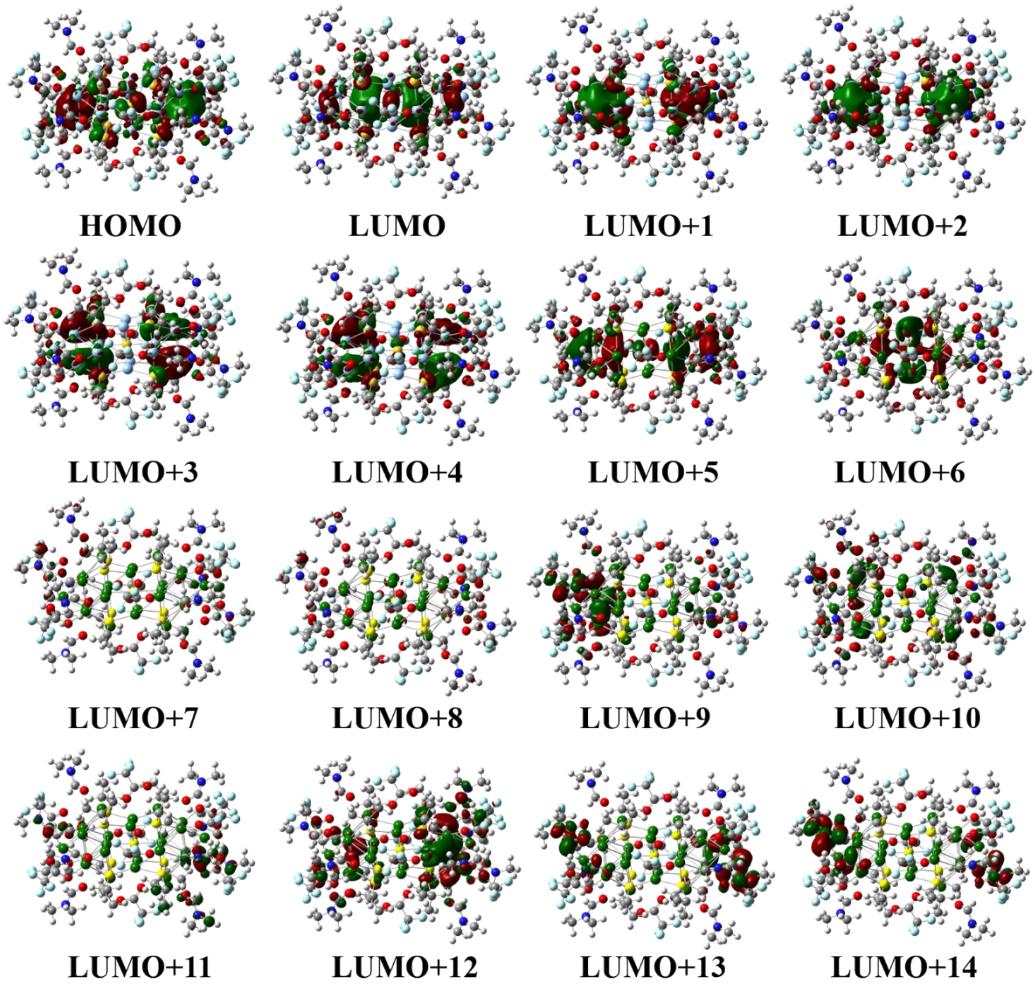

Fig. S20 Frontier orbital diagrams (HOMO, LUMO, and LUMO+1 to LUMO+14) of Ag_{24}.

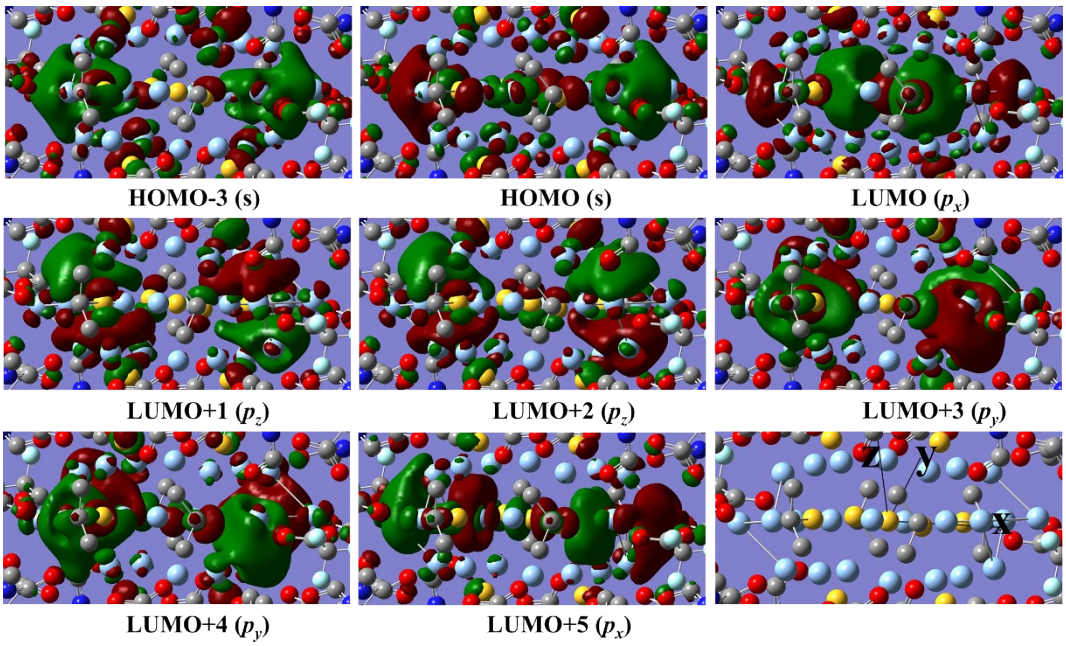

Fig. S21 The local position zoom of superatomic orbitals of Ag_{24}.

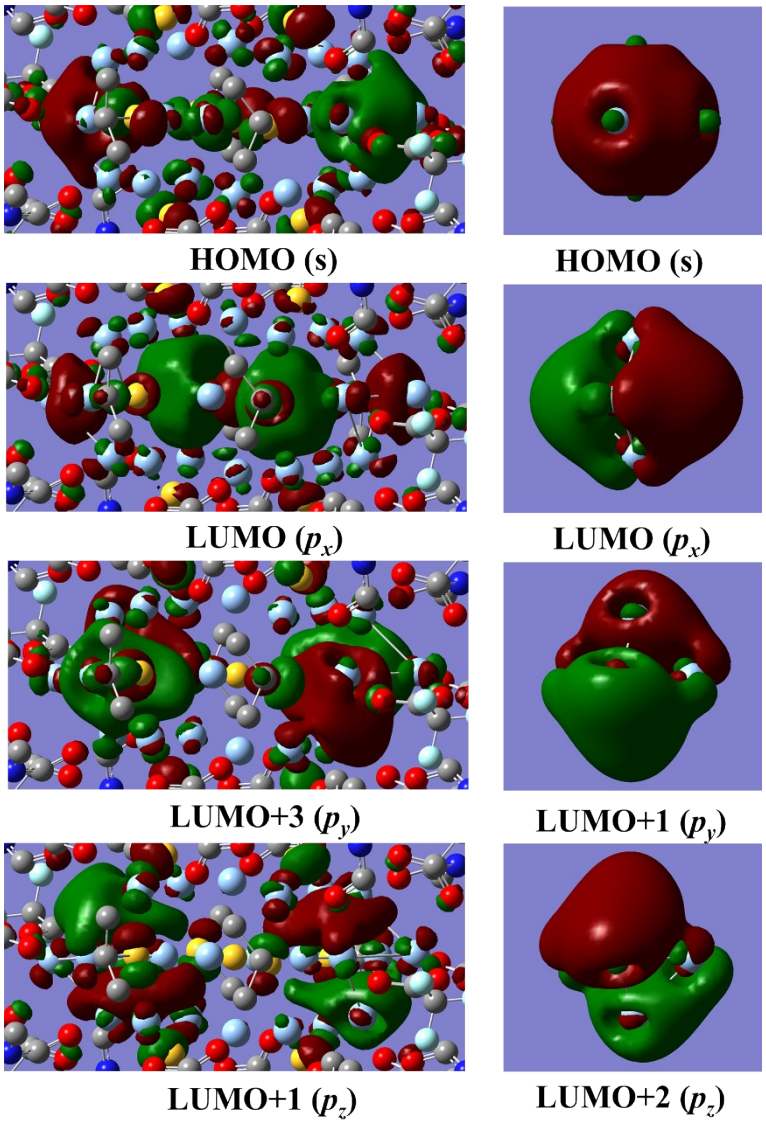

Fig. S22 The superatomic orbitals of $\mathbf{Ag_{24}}$ (left) and superatomic orbitals of the highly positively charged core Ag_6^{4+} established by removing the ligands of $\mathbf{Ag_{24}}$ (right).

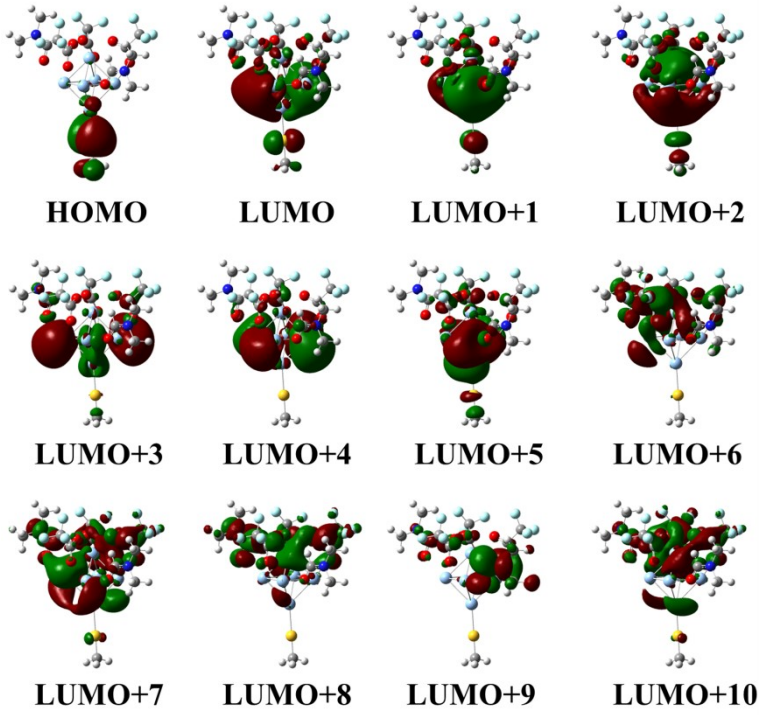

Fig. S23 Frontier orbital diagrams (HOMO, LUMO, and LUMO+1 to LUMO+10) of $Ag_6(SCH_3)(CF_3COO)_3(DMF)_2$.

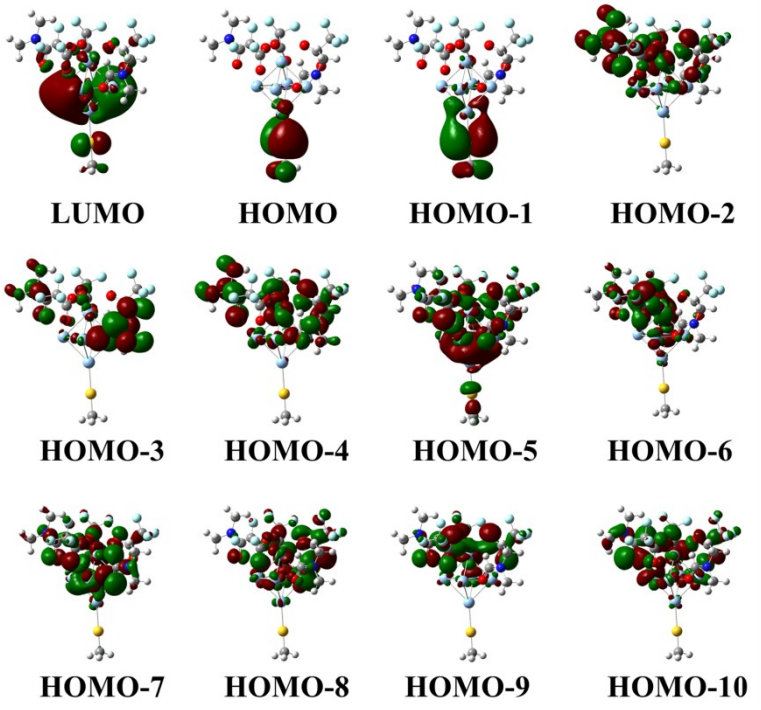

Fig. S24 Frontier orbital diagrams (HOMO, LUMO, and HOMO-1 to HOMO-10) of $Ag_6(SCH_3)(CF_3COO)_3(DMF)_2$.

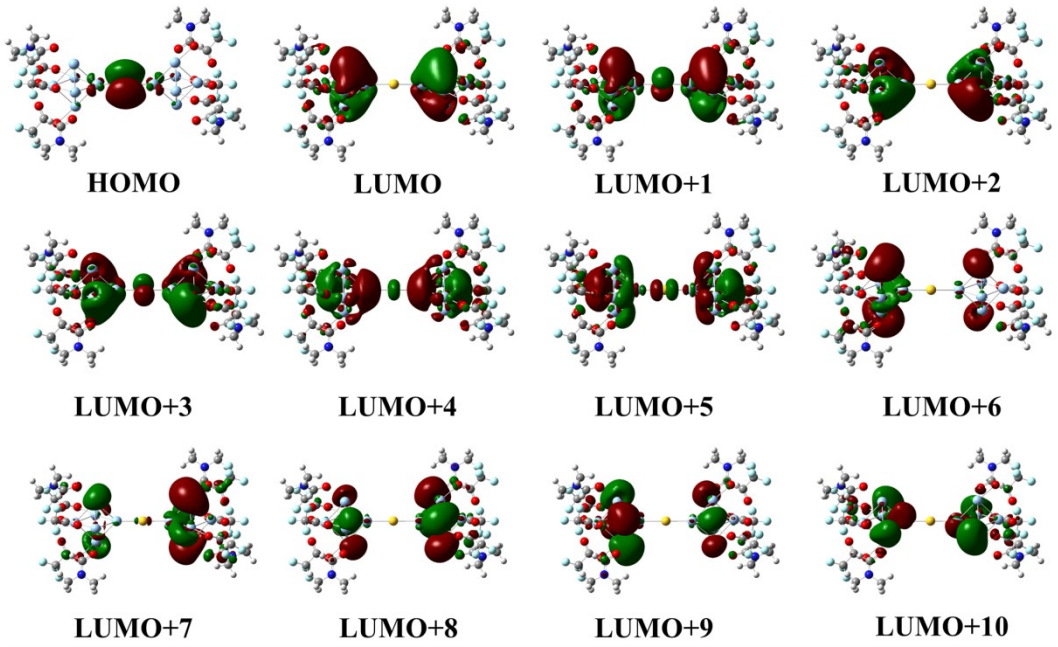

Fig. S25 Frontier orbital diagrams (HOMO, LUMO, and LUMO+1 to LUMO+10) of S@{$Ag_6(CF_3COO)_3(DMF)_2$}$_2$.

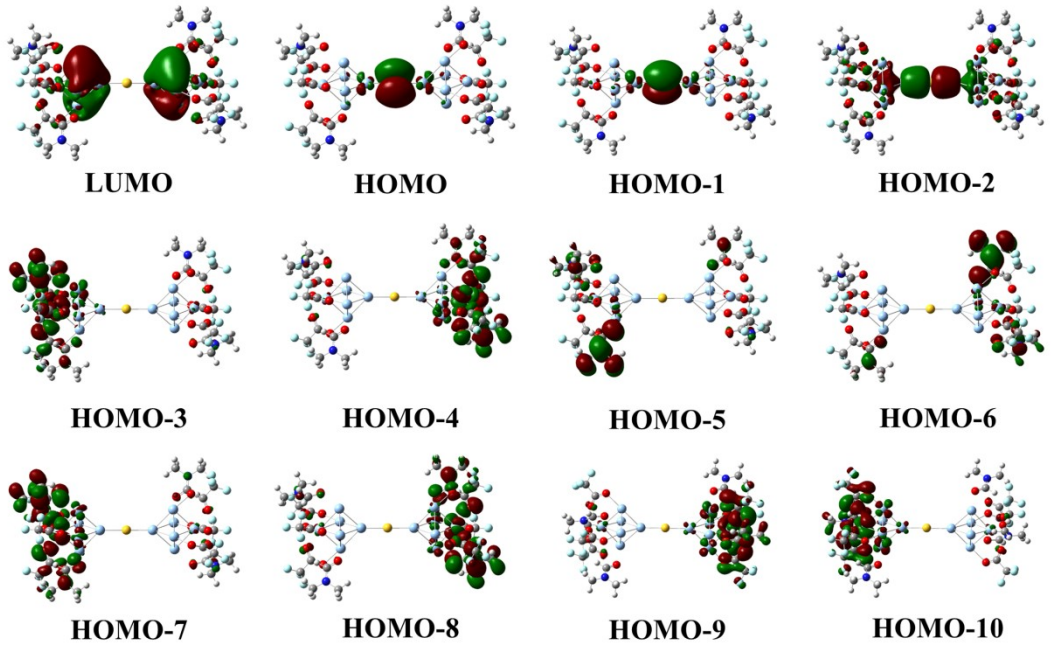

Fig. S26 Frontier orbital diagrams (HOMO, LUMO, and HOMO-1 to HOMO-10) of S@{$Ag_6(CF_3COO)_3(DMF)_2$}$_2$.

3.6 Characterization of transformation process from Ag_{24} to Ag_{70}

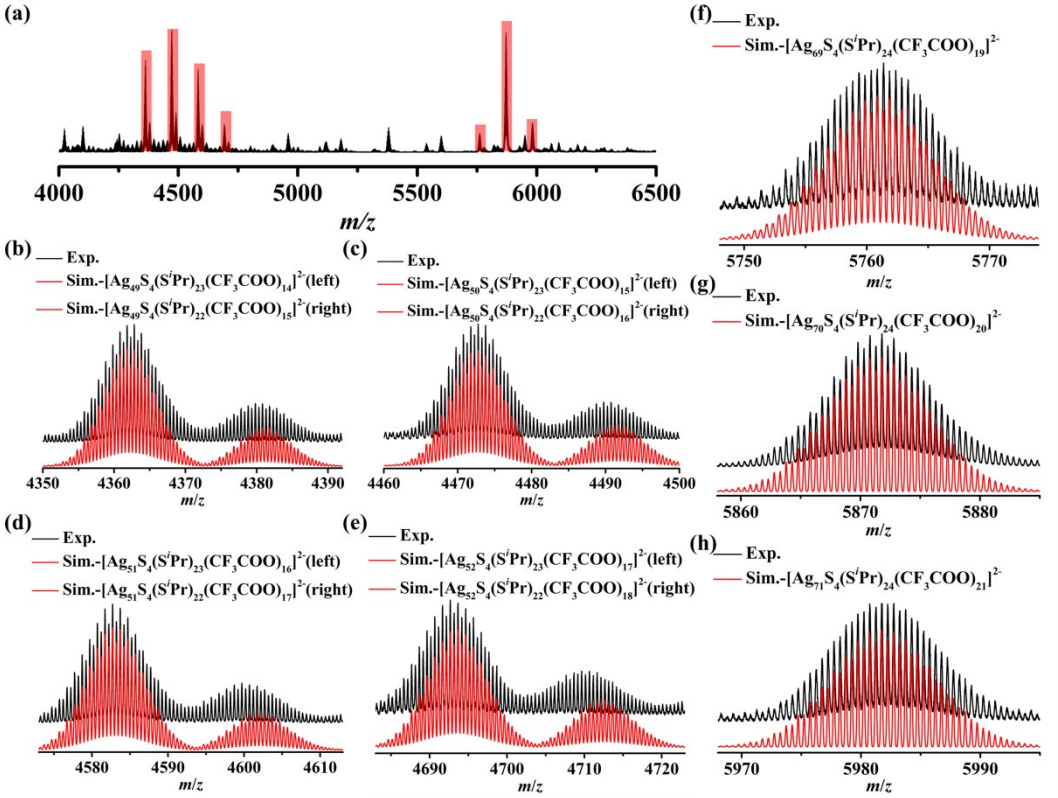

Fig. S27 (a) Negative ion mode ESI-MS in range of m/z = 4000−6500 of **Ag_{24}** dissolved in MeOH. Experimental (Exp.) and simulated (Sim.) mass spectra of the isotopic envelopes for $[Ag_{49}S_4(S^iPr)_{23}(CF_3COO)_{14}]^{2-}$ and $[Ag_{49}S_4(S^iPr)_{22}(CF_3COO)_{15}]^{2-}$ (b), $[Ag_{50}S_4(S^iPr)_{23}(CF_3COO)_{15}]^{2-}$ and $[Ag_{50}S_4(S^iPr)_{22}(CF_3COO)_{16}]^{2-}$ (c), $[Ag_{51}S_4(S^iPr)_{23}(CF_3COO)_{16}]^{2-}$ and $[Ag_{51}S_4(S^iPr)_{22}(CF_3COO)_{17}]^{2-}$ (d), $[Ag_{52}S_4(S^iPr)_{23}(CF_3COO)_{17}]^{2-}$ and $[Ag_{52}S_4(S^iPr)_{22}(CF_3COO)_{18}]^{2-}$ (e), $[Ag_{69}S_4(S^iPr)_{24}(CF_3COO)_{19}]^{2-}$ (f), $[Ag_{70}S_4(S^iPr)_{24}(CF_3COO)_{20}]^{2-}$ (g), $[Ag_{70}S_4(S^iPr)_{24}(CF_3COO)_{20}]^{2-}\cdot CF_3COOAg$ (h).

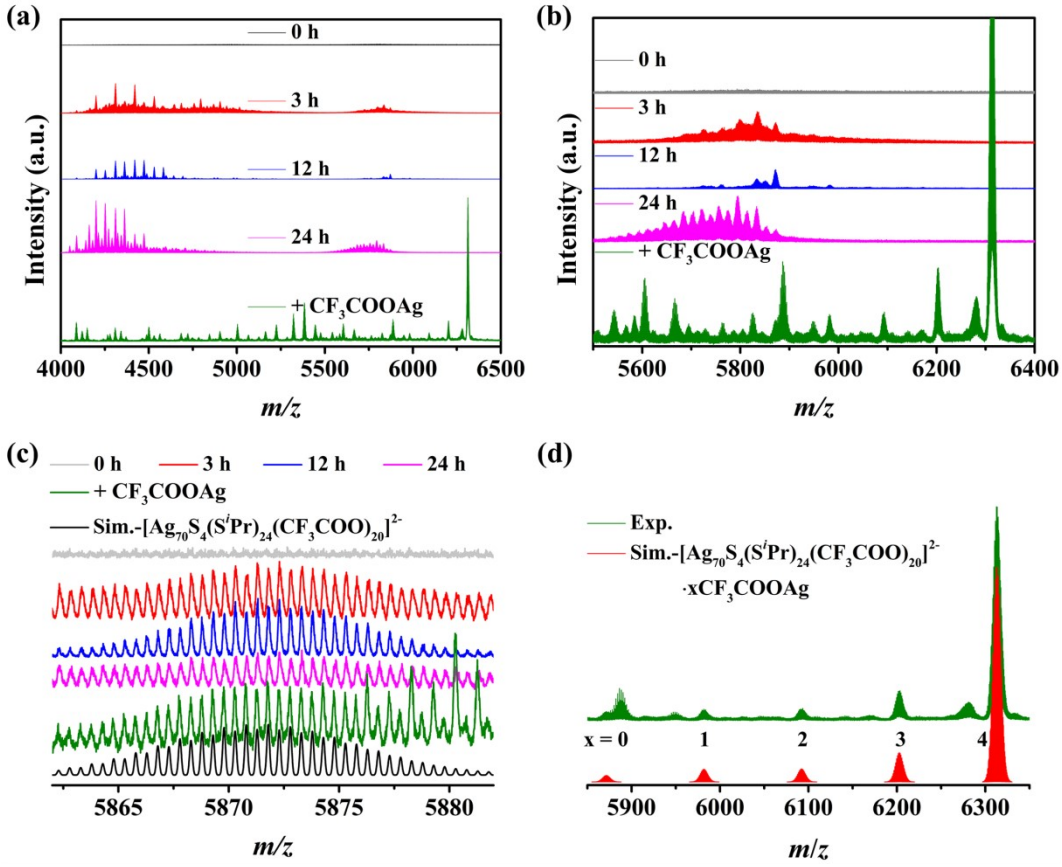

Fig. S28 (a, b) Time-dependent negative ion mode ESI-MS in range of *m*/*z* = 4000−6500 (a) and 5500−6400 (b) of $\mathbf{Ag_{24}}$ dissolved in DMF for tracking the transformation process from $\mathbf{Ag_{24}}$ to $\mathbf{Ag_{70}}$. And ESI-MS data of $\mathbf{Ag_{24}}$ dissolved in DMF containing a mount of CF_3COOAg salt as a comparison. (c, d) Experimental (Exp.) and simulated (Sim.) mass spectra of the isotopic envelopes for $[Ag_{70}S_4(S^iPr)_{24}(CF_3COO)_{20}]^{2-}$ and $[Ag_{70}S_4(S^iPr)_{24}(CF_3COO)_{20}]^{2-}\cdot(0\text{-}4)CF_3COOAg$.

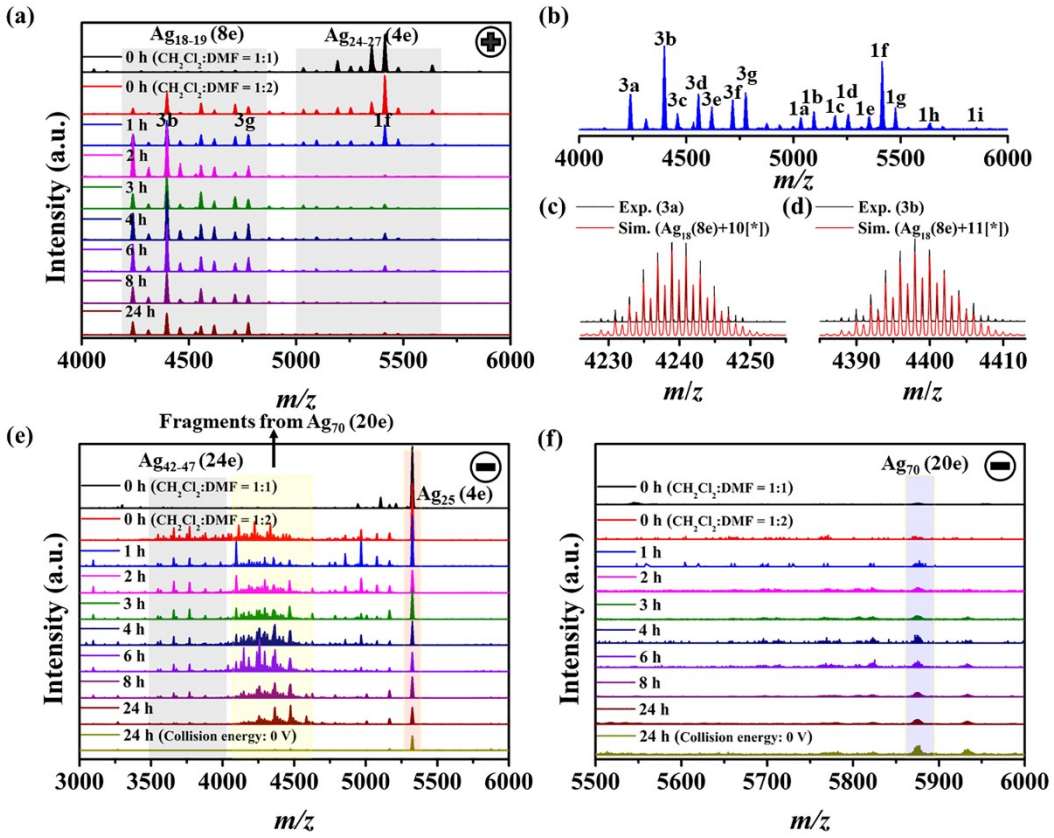

Fig. S29 Time-dependent ESI-MS spectra from $\mathbf{Ag_{24}}$ to $\mathbf{Ag_{70}}$ dissolved in mixture solvent (CH_2Cl_2: DMF = 1:2). (a) Time-dependent position ion mode ESI-MS (collision energy: 2 V) in range of *m*/*z* = 4000–6000 of $\mathbf{Ag_{24}}$ for tracking the transformation process from $\mathbf{Ag_{24}}$ to $\mathbf{Ag_{70}}$. (b) ESI-MS data after $\mathbf{Ag_{24}}$ dissolved in mixture solvent (CH_2Cl_2 : DMF = 1 : 2) for one hour. (c) Time-dependent position ion mode ESI-MS (collision energy: 2 V) in range of *m*/*z* = 3000–6000 of $\mathbf{Ag_{24}}$ for tracking the transformation process from $\mathbf{Ag_{24}}$ to $\mathbf{Ag_{70}}$. (d) Time-dependent position ion mode ESI-MS (collision energy: 2 V) in range of *m*/*z* = 5500–6000 of $\mathbf{Ag_{24}}$ for tracking the transformation process from $\mathbf{Ag_{24}}$ to $\mathbf{Ag_{70}}$. Note: [*] = $[NH_2(CH_3)_2][CF_3COO]$.

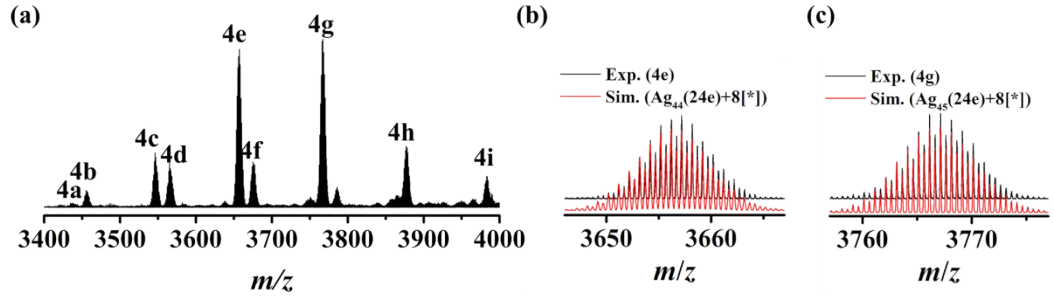

Fig. S30 (a) ESI-MS data (collision energy: 2 V) in range of *m*/*z* = 3400–4000 after $\mathbf{Ag_{24}}$ dissolved in mixture solvent (CH_2Cl_2 : DMF = 1 : 2) for three hour, highlighting the **4a**–**4i** corresponding to the $\{[NH_2(CH_3)_2]_8[Ag_{42+x}S_4(S^iPr)_{11}(CF_3COO)_{9+x}]\}^{2-}$ (x = 0–5) peaks.

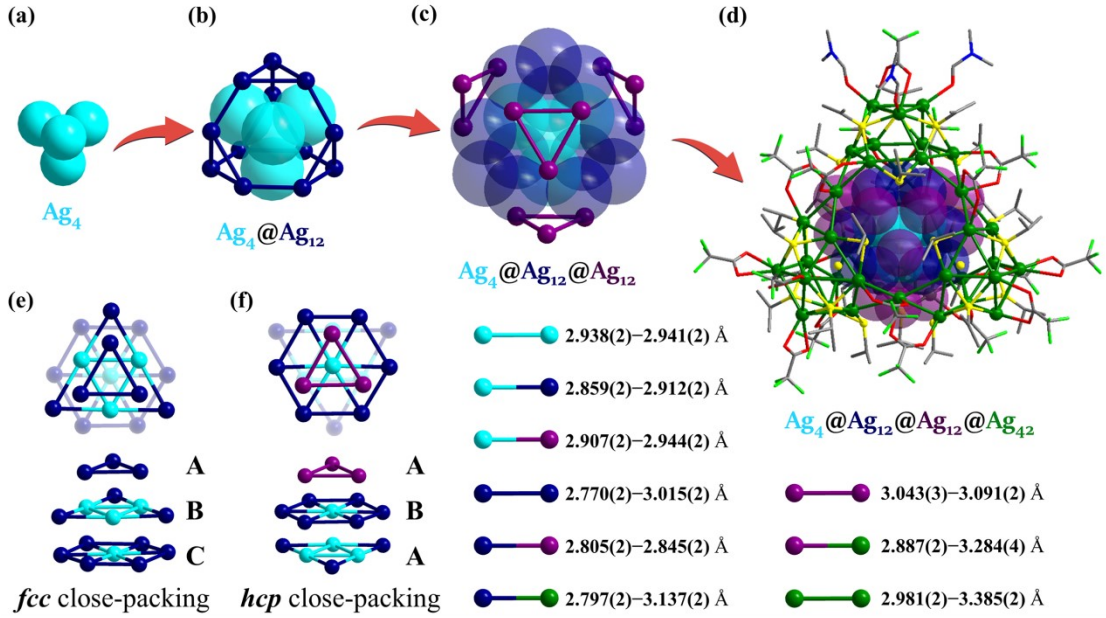

Fig. S31 The crystal structure of **Ag$_{70}$** ($[Ag_{70}S_4(S^iPr)_{24}(CF_3COO)_{20}]^{2-}$) with a core-shell metal arrangement ($Ag_4@Ag_{12}@Ag_{12}@Ag_{42}$). (a) Innermost Ag_4 tetrahedron. (b) First-shell $Ag_{12}S_4$ tetrahedron. (c) Second-shell truncated Ag_{12} tetrahedron. (d) Outermost-shell doubly truncated Ag_{42} tetrahedron. (e) ABC stacking of Ag atoms in $Ag_4@Ag_{12}$ core, identified as *fcc* close-packing. (f) ABA stacking of Ag atoms in $Ag_4@Ag_{12}@Ag_{12}$ core, identified as *hcp* close-packing. Atom color codes: turquoise/dark blue/violet/green, Ag; yellow, S; red, O; bright green, F; blue, N; grey, C. All hydrogen atoms are omitted for clarity.

Section S4. Supplementary Tables

Table S1. Crystal data collection and structure refinements.

	Ag_{14}	Ag_{24}	Ag_{24}-C_2F_5
CCDC number	2182448	2182449	2182450
Empirical formula	$C_{52}H_{84}Ag_{14}F_{24}N_6O_{22}S_6$	$C_{68}H_{112}Ag_{24}F_{30}N_8O_{28}S_9$	$C_{62}H_{77}Ag_{24}F_{50}N_5O_{25}S_9$
Formula weight	3303.79	4937.07	5119.70
Temperature (K)	200.00(10)	200.00(10)	200.00(10)
Wavelength (Å)	1.54184	0.71073	1.54184
Crystal system	monoclinic	triclinic	triclinic
Space group	$C2/c$	$P\bar{1}$	$P\bar{1}$
***a* (Å)**	21.4916(4)	14.2139(5)	14.9116(3)
***b* (Å)**	18.1316(4)	15.6549(4)	16.3962(2)
***c* (Å)**	23.7184(4)	17.3498(6)	18.2438(3)
***α* (°)**	90	94.120(2)	97.091(1)
***β* (°)**	91.945(2)	110.998(3)	112.841(2)
***γ* (°)**	90	104.208(2)	104.162(1)
***V* (Å^3)**	9237.2(3)	3439.1(2)	3864.9(2)
Z	4	1	1
ρ_{calc} (g/cm^3)	2.376	2.384	2.200
μ (mm^{-1})	25.507	3.562	25.887
***F* (000)**	6336.0	2342.0	2406.0
Crystal size (mm)	0.12 × 0.11 × 0.10	0.10 × 0.05 × 0.05	0.08 × 0.07 × 0.06
Radiation type	Cu $K\alpha$	Mo $K\alpha$	Cu $K\alpha$
2θ range for data collection (°)	7.32 to 132.998	4.052 to 58.676	5.42 to 149.168
Limiting indices	$-25 \le h \le 23$, $-21 \le k \le 21$, $-28 \le l \le 28$	$-19 \le h \le 19$, $-21 \le k \le 18$, $-22 \le l \le 23$	$-18 \le h \le 18$, $-20 \le k \le 17$, $-22 \le l \le 21$
Reflections collected	13218	54748	33822
Independent reflections	13218 [R_{int} = 0.3401, R_{sigma} = 0.0280]	15940 [R_{int} = 0.0456, R_{sigma} = 0.0512]	15003 [R_{int} = 0.0598, R_{sigma} = 0.0726]
Data/restraints/parameters	13218/176/629	15940/1065/1093	15003/5120/1424
Goodness-of-fit on F^2	1.071	1.050	1.030
Final R indices [$I>2\sigma(I)$]	R_1 = 0.1149, wR_2 = 0.3121	R_1 = 0.0727, wR_2 = 0.2291	R_1 = 0.0995, wR_2 = 0.3071
R indices [all data]	R_1 = 0.1220, wR_2 = 0.3217	R_1 = 0.1009, wR_2 = 0.2493	R_1 = 0.1286, wR_2 = 0.3306
Largest diff. peak/hole / e Å^{-3}	2.88/-3.67	2.15/-1.67	1.90/-1.59

Table S2. The distances (Å) of Ag···Ag, Ag−S, and Ag−O in **Ag_{14}**.

Ag1···Ag2	3.0044(19)	Ag1···Ag5	3.335(2)	Ag1···Ag7[1]	2.9512(19)
Ag2···Ag3	3.072(2)	Ag2···Ag6[1]	2.9985(19)	Ag2···Ag7[1]	2.993(2)
Ag3···Ag4	2.992(2)	Ag3···Ag6[1]	3.0747(19)	Ag3···Ag7	3.001(2)
Ag5···Ag4	2.936(2)	Ag7···Ag4	2.907(2)	Ag5···Ag6	2.835(2)
Ag1−S1	2.486(5)	Ag1−S3[1]	2.520(4)	Ag2−S1	2.533(5)
Ag2−S2[1]	2.621(4)	Ag3−S1	2.527(5)	Ag3−S3	2.550(4)
Ag4−S1	2.518(5)	Ag4−S2	2.665(4)	Ag5−S2	2.682(4)
Ag6−S2	2.633(4)	Ag6−S3[1]	2.502(5)	Ag7−S2	2.474(4)
Ag7−S3	2.461(4)				
Ag1−O4	2.342(16)	Ag1−O9	2.492(15)	Ag2−O2	2.50(2)
Ag2−O3	2.381(16)	Ag3−O1	2.39(2)	Ag3−O5	2.397(16)
Ag4−O6	2.243(16)	Ag4−O10	2.511(13)	Ag5−O7	2.309(17)
Ag5−O9	2.41(2)	Ag5−O10	2.478(15)	Ag6−O8	2.268(16)
Ag7−O11	2.28(2)				
Symmetry code: [1]3/2-x, 3/2-y, 1-z.					

Table S3. The distances (Å) of Ag···Ag, Ag−S, and Ag−O in **Ag_{24}**.

Ag1A···Ag2	2.739(8)	Ag1B···Ag2	2.802(13)	Ag2···Ag3	2.7781(11)
Ag1A···Ag3	2.779(9)	Ag1B···Ag3	2.94(2)	Ag2···Ag4	2.7774(11)
Ag1A···Ag5	2.820(9)	Ag1B···Ag5	2.827(10)	Ag2···Ag5	2.8023(12)
Ag1A···Ag6	2.750(9)	Ag1B···Ag6	2.857(18)	Ag3···Ag4	2.8306(12)
Ag1A···Ag9	3.043(8)	Ag1B···Ag9	3.134(16)	Ag3···Ag6	2.8436(11)
Ag1A···Ag10	3.073(10)	Ag1B···Ag10	3.003(13)	Ag3···Ag8	3.1452(12)
Ag4···Ag5	2.8213(13)	Ag5···Ag6	2.8545(11)	Ag3···Ag9	3.0768(12)
Ag4···Ag6	2.8173(11)	Ag5···Ag7	3.0907(13)	Ag6···Ag7	3.2381(12)
Ag4···Ag7	3.1108(13)	Ag5···Ag10	3.1103(12)	Ag6···Ag8	3.2293(12)
Ag4···Ag8	3.1692(12)	Ag8···Ag12[1]	3.363(5)	Ag6···Ag9	3.2268(12)
Ag7···Ag12[1]	3.354(4)	Ag8···Ag1[1]	3.226(10)	Ag6···Ag10	3.2124(12)
Ag7···Ag1[1]	3.350(7)	Ag9···Ag11[1]	3.2245(15)	Ag6···Ag1[1]	3.31(2)
Ag10···Ag11	3.3471(16)	Ag10···Ag1	3.351(7)		
Ag1−S4	2.568(14)	Ag1−S5	2.34(3)	Ag1−S21	2.542(10)
Ag1A−S4	2.568(9)	Ag1B−S	2.533(10)	Ag3−S1	2.535(3)
Ag4−S2	2.547(2)	Ag5−S3	2.574(3)	Ag6−S5	2.5265(7)
Ag7−S2	2.522(3)	Ag8−S1	2.504(3)	Ag9−S1	2.521(3)
Ag7−S3	2.514(3)	Ag8−S2	2.510(3)	Ag9−S4	2.511(3)
Ag10−S3	2.523(3)	Ag11−S1[1]	2.457(3)	Ag11−S3	2.456(3)
Ag10−S4	2.521(3)	Ag11−S5	2.6191(12)	Ag12−S2[1]	2.388(5)
Ag12−S4	2.387(4)	Ag12···S5	2.938(17)		
Ag1A−O8	2.32(2)	Ag1B−O	2.23(3)	Ag3−O7	2.249(11)
Ag2−O3	2.372(12)	Ag4−O11	2.29(2)	Ag4−O13	2.29(2)
Ag2−O4	2.351(10)	Ag5−O10	2.260(12)	Ag5−O20	2.48(2)
Ag2−O5	2.369(10)	Ag7−O2[1]	2.511(15)	Ag7−O12	2.39(2)
Ag8−O9	2.348(15)	Ag8−O17	2.30(4)	Ag9−O6	2.333(12)
Ag9−O18	2.452(10)	Ag10−O1[1]	2.584(10)	Ag10−O14[1]	2.27(3)
Ag10−O19	2.46(3)				
Symmetry code: [1]1-x, 1-y, 1-z.					

Table S4. The Ag···Ag distances of Ag_6 octahedral core in Ag cluster reported.

	Formula	Ag···Ag distances (Å)	Average (Å)	Ref.
	$TBA_8[Ag_6(H_2SiW_{10}O_{36})_2]\cdot 5H_2O$	2.715(2)–2.858(2)	2.764	[9]
	$[Ag(CH_3CN)]_2[Ag_6Ti_{16}O_{22}(PhCOO)_{26}(CH_3CN)_2]$	2.690(2)–2.776(2)	2.752	[10]
	$Ag_6Ti_{16}O_{20}(PhCOO)_{24}(CH_3COO)_4(CH_3CN)_2$	2.731(3)–2.741(2)	2.734	[10]
	$[Ag_{14}(C_2B_{10}H_{10}S_2)_6(CH_3CN)_8]\cdot 4CH_3CN$	2.745(2)–2.774(1)	2.764	[11]
	$[Ag_6@(MoO_4)_7@Ag_{56}(MoO_4)_2(^iPrS)_{28}(p\text{-}TOS)_{14}(DMF)_4]$	2.659(5)–2.852(4)	2.756	[12]
	$[Ag_{14}(pntp)_{10}(dpph)_4Cl_2]$	2.800(1)–2.853(1)	2.821	[13]
	$[Ag_{14}(SC_6H_3F_2)_{12}(PPh_3)_8]$	2.814(2)–2.852(2)	2.838	[14]
Ag_6^{4+}	$[Ag_{14}(SPh(CF_3)_2)_{12}(PPh_3)_4(DMF)_4]$	2.834(1)–2.865(1)	2.852	[15]
	$[Ag_{14}(NLA)_6(PPh_3)_8]$	2.842(1)–2.846(1)	2.844	[16]
	$[Ag_{14}(FBT)_{12}(PPh_3)_8]$	2.832(2)–2.847(1)	2.840	[17]
	$[Ag_6@(MoO_4)_7@Ag_{60}(MoO_4)_2(^iPrS)_{28}(PhCOO)_{18}(CH_3OH)_2]$	2.659(6)–2.855(3)	2.764	[18]
	$[Ag_6@(CrO_4)_8@Ag_{52}(^iPrS)_{30}(DMF)_{14}]\cdot 10BF_4\cdot 2DMF$	2.773(1)–2.862(1)	2.818	[19]
	$[TBA_8H_6Ag_6(SiW_9O_{33})_2(DMF)]^{2+}$	2.685(2)–2.847(1)	2.771	[20]
	$(TBA)_2\{Ag_6Ti_6(Sal)_x(L1)_6(HL1)_{6-x}\}$ (x = 0-3)	2.760(1)–2.813(1)	2.784	[21]
	$S@Ag_{24}(S^iPr)_8(CF_3COO)_{10}(DMF)_{10}$	**2.767(4)–2.853(3)**	**2.805**	**This work**
	$[Ag_6S_4@Ag_{36}(^tBuPhS)_{24}(CF_3COO)_6(H_2O)_{12}]\cdot 4CF_3COO$	2.928(4)–2.968(3)	2.941	[22]
	$[Ag_6Se_4@Ag_{36}(^tBuPhS)_{24}(CF_3COO)_6(H_2O)_{12}]\cdot 4CF_3COO$	2.936(3)–2.984(3)	2.965	[22]
Ag_6^{6+}	$[Ag_6S_4@Ag_{36}Ti_4(S^iPr)_{18}(SA)_{12}(SO_4)_4]\cdot 8MeOH$	2.845(1)–3.106(1)	2.961	[23]
	$[Ag_6L_6/D_6]$	2.957(2)–3.332(2)	3.210	[24]
	$[Ag_6PL_6/PD_6]$	2.948(2)–3.442(2)	3.136	[24]

Hpntp = p-nitrothiophenol; dpph = 1,6-bis(diphenylphosphino)hexane; NLA = D,L-6,8-thioctamide; FBT = 4-fluorothiophenol; SA = salicylate; L/D = (S/R)-4-isopropylthiazolidine-2-thione; PL/PD = (S/R)-2-phenylglycinol; TBA^+ = tetrabutylamine; H_3L1 = 2,6-dihydroxybenzoic acid

Table S5. The assigned formula of species found in ESI-MS (**Ag_{24}** in CH_2Cl_2/DMF (*v*:*v* = 1:1); Declustering potential: 40 V; Collision energy: 2 V). Note: [*] = $[NH_2(CH_3)_2][CF_3COO]$.

Peak	Formula	Cal.	Exp.
1a (Ag_{24}(4e)+5[*])	$\{[NH_2(CH_3)_2]_5Ag_{24}S(S^iPr)_8(CF_3COO)_{14}]\}^+$	5034.02	5034.02
1b (Ag_{25}(4e)+4[*])	$\{[NH_2(CH_3)_2]_4Ag_{25}S(S^iPr)_8(CF_3COO)_{14}]\}^+$	5096.86	5096.88
1c (Ag_{24}(4e)+6[*])	$\{[NH_2(CH_3)_2]_6Ag_{24}S(S^iPr)_8(CF_3COO)_{15}]\}^+$	5193.08	5193.11
1d (Ag_{25}(4e)+5[*])	$\{[NH_2(CH_3)_2]_5Ag_{25}S(S^iPr)_8(CF_3COO)_{15}]\}^+$	5255.91	5255.91
1e (Ag_{24}(4e)+7[*])	$\{[NH_2(CH_3)_2]_7Ag_{24}S(S^iPr)_8(CF_3COO)_{16}]\}^+$	5352.13	5352.16
1f (Ag_{25}(4e)+6[*])	$\{[NH_2(CH_3)_2]_6Ag_{25}S(S^iPr)_8(CF_3COO)_{16}]\}^+$	5414.97	5414.97
1g (Ag_{26}(4e)+5[*])	$\{[NH_2(CH_3)_2]_5Ag_{26}S(S^iPr)_8(CF_3COO)_{16}]\}^+$	5475.80	5475.81
1h (Ag_{26}(4e)+6[*])	$\{[NH_2(CH_3)_2]_6Ag_{26}S(S^iPr)_8(CF_3COO)_{17}]\}^+$	5634.86	5634.91
1i (Ag_{27}(4e)+6[*])	$\{[NH_2(CH_3)_2]_6Ag_{27}S(S^iPr)_8(CF_3COO)_{18}]\}^+$	5856.75	5856.77
2a (Ag_{24}(4e)+3[*])	$\{[NH_2(CH_3)_2]_3[Ag_{24}S(S^iPr)_8(CF_3COO)_{14}]\}^-$	4941.89	4941.87
2b Ag_{24}(4e)+4[*])	$\{[NH_2(CH_3)_2]_4[Ag_{24}S(S^iPr)_8(CF_3COO)_{15}]\}^-$	5100.94	5100.93
2c Ag_{25}(4e)+3[*])	$\{[NH_2(CH_3)_2]_3[Ag_{25}S(S^iPr)_8(CF_3COO)_{15}]\}^-$	5163.78	5163.76
2d Ag_{25}(4e)+4[*])	$\{[NH_2(CH_3)_2]_4[Ag_{25}S(S^iPr)_8(CF_3COO)_{16}]\}^-$	5322.83	5322.83
2e (Ag_{26}(4e)+4[*])	$\{[NH_2(CH_3)_2]_4[Ag_{26}S(S^iPr)_8(CF_3COO)_{17}]\}^-$	5542.72	5542.72

Table S6. The assigned formula of species found in ESI-MS (**Ag_{24}** in CH_2Cl_2/^{i}PrOH (*v*:*v* = 4:1); Declustering potential: 40 V; Collision energy: 2 V). Note: [*] = $[NH_2(CH_3)_2][CF_3COO]$.

Peak	Formula	Cal.	Exp.
2f (Ag_{24}(4e)+0[*])	$\{[NH_2(CH_3)_2]_0[Ag_{24}S(S^iPr)_8(CF_3COO)_{12}]\}^{2-}$	2288.86	2288.86
2g (Ag_{24}(4e)+1[*])	$\{[NH_2(CH_3)_2]_1[Ag_{24}S(S^iPr)_8(CF_3COO)_{13}]\}^{2-}$	2368.39	2368.39
2h (Ag_{25}(4e)+0[*])	$\{[NH_2(CH_3)_2]_0[Ag_{25}S(S^iPr)_8(CF_3COO)_{13}]\}^{2-}$	2399.81	2399.82
2i (Ag_{24}(4e)+2[*])	$\{[NH_2(CH_3)_2]_2[Ag_{24}S(S^iPr)_8(CF_3COO)_{14}]\}^{2-}$	2447.91	2447.92
2j (Ag_{25}(4e)+1[*])	$\{[NH_2(CH_3)_2]_1[Ag_{25}S(S^iPr)_8(CF_3COO)_{14}]\}^{2-}$	2479.33	2479.34
2k (Ag_{24}(4e)+3[*])	$\{[NH_2(CH_3)_2]_3[Ag_{24}S(S^iPr)_8(CF_3COO)_{15}]\}^{2-}$	2527.44	2527.45
2l (Ag_{25}(4e)+2[*])	$\{[NH_2(CH_3)_2]_2[Ag_{25}S(S^iPr)_8(CF_3COO)_{15}]\}^{2-}$	2558.86	2558.86
2m (Ag_{25}(4e)+3[*])	$\{[NH_2(CH_3)_2]_3[Ag_{25}S(S^iPr)_8(CF_3COO)_{16}]\}^{2-}$	2638.38	2638.39
2n (Ag_{25}(4e)+4[*])	$\{[NH_2(CH_3)_2]_4[Ag_{25}S(S^iPr)_8(CF_3COO)_{17}]\}^{2-}$	2717.91	2717.92

Table S7. Transition energy, oscillator strength, and orbital contributions of the strongest electronic excitations of Ag_{24}.

Wavelength (nm)	Osc. Strength	Major contribs
406.4760889	0.0165	H-2->LUMO (27%), H-1->LUMO (65%)
402.9095822	0.1471	H-2->LUMO (33%), H-1->LUMO (12%), HOMO->LUMO (42%)
393.6603799	0.4173	H-2->LUMO (34%), H-1->LUMO (10%), HOMO->LUMO (50%)
369.8786893	0.0233	H-5->LUMO (22%), H-3->LUMO (57%), HOMO->L+1 (11%)
369.4048108	0.1309	H-3->L+2 (10%), HOMO->L+1 (65%)
360.962317	0.0446	H-1->L+1 (74%)
357.5376666	0.0347	H-2->L+1 (68%), HOMO->L+3 (10%)
356.3456346	0.0279	H-7->LUMO (21%), H-1->L+2 (23%), HOMO->L+3 (12%)
356.0488675	0.114	H-2->L+1 (10%), H-1->L+2 (13%), HOMO->L+3 (46%)
348.0331704	0.0224	H-4->L+1 (35%), H-1->L+3 (44%)
344.4077242	0.0252	H-2->L+3 (69%)
339.3085294	0.011	H-11->LUMO (45%), H-6->L+1 (28%)
338.0226741	0.0607	H-11->LUMO (28%), H-6->L+1 (32%)
334.0698317	0.049	H-4->L+3 (73%)
325.5266538	0.0438	H-12->LUMO (17%), H-6->L+4 (11%), H-3->L+2 (28%)
325.0061252	0.0343	H-12->LUMO (18%), H-3->L+2 (23%)
323.6317845	0.046	H-14->L+1 (10%), H-8->L+2 (12%), H-7->L+2 (27%), H-5->L+2 (22%)
318.3467792	0.0123	H-14->LUMO (60%), H-13->LUMO (14%)
314.8383358	0.1055	H-3->L+4 (32%)
312.9864858	0.0624	H-8->L+2 (16%), H-5->L+2 (15%), H-3->L+4 (12%)
311.9391552	0.0152	H-7->L+4 (42%)
310.1211552	0.0571	H-15->LUMO (56%), H-10->L+2 (10%)
308.6004994	0.0391	H-15->LUMO (20%), H-13->L+1 (18%), H-12->L+2 (13%), H-10->L+2 (15%)
307.8189996	0.0146	H-16->LUMO (37%)
305.5206541	0.0151	H-10->L+4 (16%)
303.5607978	0.0374	H-8->L+4 (26%), H-5->L+4 (22%)
303.0043908	0.04	H-11->L+1 (30%), H-10->L+4 (15%)
300.6385467	0.0368	H-11->L+1 (16%), H-9->L+2 (38%)

Table S8. The assigned formula of species found in ESI-MS (**Ag_{24}** dissolved in mixture solvent (CH_2Cl_2 : DMF = 1 : 2) for one hour; Declustering potential: 40 V; Collision energy: 2 V). Note: [*] = $[NH_2(CH_3)_2][CF_3COO]$.

Peak	Formula	Cal.	Exp.
3a **(Ag_{18}(8e)+10[*])**	$\{[NH_2(CH_3)_2]_{10}Ag_{18}S(S^iPr)_5(CF_3COO)_{12}(DMF)]\}^+$	4238.93	4238.94
3b **(Ag_{18}(8e)+11[*])**	$\{[NH_2(CH_3)_2]_{11}Ag_{18}S(S^iPr)_5(CF_3COO)_{13}(DMF)]\}^+$	4397.98	4397.97
3c **(Ag_{19}(8e)+10[*])**	$\{[NH_2(CH_3)_2]_{10}Ag_{19}S(S^iPr)_5(CF_3COO)_{13}(DMF)]^+$	4460.82	4460.78
3d **(Ag_{18}(8e)+12[*])**	$\{[NH_2(CH_3)_2]_{12}Ag_{18}S(S^iPr)_5(CF_3COO)_{14}(DMF)]\}^+$	4557.03	4556.98
3e **(Ag_{19}(8e)+11[*])**	$\{[NH_2(CH_3)_2]_{11}Ag_{19}S(S^iPr)_5(CF_3COO)_{14}(DMF)]\}^+$	4619.87	4619.82
3f **(Ag_{18}(8e)+13[*])**	$\{[NH_2(CH_3)_2]_{13}Ag_{18}S(S^iPr)_5(CF_3COO)_{15}(DMF)]\}^+$	4716.08	4716.02
3g **(Ag_{19}(8e)+12[*])**	$\{[NH_2(CH_3)_2]_{12}Ag_{19}S(S^iPr)_5(CF_3COO)_{15}(DMF)]\}^+$	4778.92	4778.86

Table S9. The assigned formula of species found in ESI-MS (**Ag_{24}** dissolved in mixture solvent (CH_2Cl_2 : DMF = 1 : 2) for three hour; Declustering potential: 40 V; Collision energy: 2 V). Note: [*] = $[NH_2(CH_3)_2][CF_3COO]$.

Peak	Formula	Cal.	Exp.
4a **(Ag_{42}(24e)+8[*])**	$\{[NH_2(CH_3)_2]_8[Ag_{42}S_4(S^iPr)_{11}(CF_3COO)_9]\}^{2-}$	3435.29	3435.30
4b **(Ag_{42}(24e)+8[*])**	$\{[NH_2(CH_3)_2]_8[Ag_{42}S_4(S^iPr)_{10}(CF_3COO)_{10}]\}^{2-}$	3454.27	3454.29
4c **(Ag_{43}(24e)+8[*])**	$\{[NH_2(CH_3)_2]_8[Ag_{43}S_4(S^iPr)_{11}(CF_3COO)_{10}]\}^{2-}$	3546.24	3546.27
4d **(Ag_{43}(24e)+8[*])**	$\{[NH_2(CH_3)_2]_8[Ag_{43}S_4(S^iPr)_{10}(CF_3COO)_{11}]\}^{2-}$	3565.22	3565.24
4e **(Ag_{44}(24e)+8[*])**	$\{[NH_2(CH_3)_2]_8[Ag_{44}S_4(S^iPr)_{11}(CF_3COO)_{11}]\}^{2-}$	3656.18	3656.20
4f **(Ag_{44}(24e)+8[*])**	$\{[NH_2(CH_3)_2]_8[Ag_{44}S_4(S^iPr)_{10}(CF_3COO)_{12}]\}^{2-}$	3675.16	3675.17
4g **(Ag_{45}(24e)+8[*])**	$\{[NH_2(CH_3)_2]_8[Ag_{45}S_4(S^iPr)_{11}(CF_3COO)_{12}]\}^{2-}$	3767.13	3767.14
4h **(Ag_{45}(24e)+8[*])**	$\{[NH_2(CH_3)_2]_8[Ag_{45}S_4(S^iPr)_{10}(CF_3COO)_{13}]\}^{2-}$	3786.11	3786.11
4i **(Ag_{46}(24e)+8[*])**	$\{[NH_2(CH_3)_2]_8[Ag_{46}S_4(S^iPr)_{11}(CF_3COO)_{13}]\}^{2-}$	3877.07	3877.07
4j **(Ag_{47}(24e)+8[*])**	$\{[NH_2(CH_3)_2]_8[Ag_{47}S_4(S^iPr)_{11}(CF_3COO)_{14}]\}^{2-}$	3988.02	3988.02

References

1 G. M. Sheldrick, *Acta Cryst. A*, 2008, **64**, 112-122.
2 O. V. Dolomanov, L. J. Bourhis, R. J. Gildea, J. A. K. Howard and H. Puschmann, *J. Appl. Crystallogr.*, 2009, **42**, 339-341.
3 (a) G. M. Sheldrick, *Acta Cryst. C*, 2015, **71**, 3-8; (b) C. B. Huebschle, G. M. Sheldrick and B. Dittrich, *J. Appl. Crystallogr.*, 2011, **44**, 1281-1284.
4 A. Spek, *Acta Cryst. D*, 2009, **65**, 148-155.
5 M. J. Frisch, G. W. Trucks, H. B. Schlegel, G. E. Scuseria, M. A. Robb, J. R. Cheeseman, G. Scalmani, V. Barone, G. A. Petersson, H. Nakatsuji, X. Li, M. Caricato, A. V. Marenich, J. Bloino, B. G. Janesko, R. Gomperts, B. Mennucci, H. P. Hratchian, J. V. Ortiz, A. F. Izmaylov, J. L. Sonnenberg, Williams, F. Ding, F. Lipparini, F. Egidi, J. Goings, B. Peng, A. Petrone, T. Henderson, D. Ranasinghe, V. G. Zakrzewski, J. Gao, N. Rega, G. Zheng, W. Liang, M. Hada, M. Ehara, K. Toyota, R. Fukuda, J. Hasegawa, M. Ishida, T. Nakajima, Y. Honda, O. Kitao, H. Nakai, T. Vreven, K. Throssell, J. A. Montgomery Jr., J. E. Peralta, F. Ogliaro, M. J. Bearpark, J. J. Heyd, E. N. Brothers, K. N. Kudin, V. N. Staroverov, T. A. Keith, R. Kobayashi, J. Normand, K. Raghavachari, A. P. Rendell, J. C. Burant, S. S. Iyengar, J. Tomasi, M. Cossi, J. M. Millam, M. Klene, C. Adamo, R. Cammi, J. W. Ochterski, R. L. Martin, K. Morokuma, O. Farkas, J. B. Foresman and D. J. Fox, Wallingford, CT, **2016**.
6 J. P. Perdew, K. Burke and M. Ernzerhof, *Phys. Rev. Lett.*, 1996, **77**, 3865-3868.
7 (a) B. P. Pritchard, D. Altarawy, B. Didier, T. D. Gibson and T. L. Windus, *J. Chem. Inf. Model.*, 2019, **59**, 4814-4820; (b) K. L. Schuchardt, B. T. Didier, T. Elsethagen, L. Sun, V. Gurumoorthi, J. Chase, J. Li and T. L. Windus, *J. Chem. Inf. Model.*, 2007, **47**, 1045-1052; (c) D. Feller, *J. Comput. Chem.*, 1996, **17**, 1571-1586; (d) F. Weigend and R. Ahlrichs, *Phys. Chem. Chem. Phys.*, 2005, **7**, 3297-3305; (e) D. Andrae, U. Häußermann, M. Dolg, H. Stoll and H. Preuß, *Theoret. Chim. Acta*, 1990, **77**, 123-141.
8 T. Lu and F. Chen, *J. Comput. Chem.*, 2012, **33**, 580-592.
9 Y. Kikukawa, Y. Kuroda, K. Suzuki, M. Hibino, K. Yamaguchi and N. Mizuno, *Chem. Commun.*, 2013, **49**, 376-378.
10 S. Chen, W. H. Fang, L. Zhang and J. Zhang, *Angew. Chem. Int. Ed.*, 2018, **57**, 11252-11256.
11 Z.-Y. Wang, M.-Q. Wang, Y.-L. Li, P. Luo, T.-T. Jia, R.-W. Huang, S.-Q. Zang and T. C. W. Mak, *J. Am. Chem. Soc.*, 2018, **140**, 1069-1076.
12 Z. Wang, H.-F. Su, M. Kurmoo, C.-H. Tung, D. Sun and L.-S. Zheng, *Nat. Commun.*, 2018, **9**, 2094.
13 X.-Q. Liang, Y.-Z. Li, Z. Wang, S.-S. Zhang, Y.-C. Liu, Z.-Z. Cao, L. Feng, Z.-Y. Gao, Q.-W. Xue, C.-H. Tung and D. Sun, *Nat. Commun.*, 2021, **12**, 4966.
14 H. Yang, J. Lei, B. Wu, Y. Wang, M. Zhou, A. Xia, L. Zheng and N. Zheng, *Chem. Commun.*, 2013, **49**, 300-302.
15 (a) G. Deng, B. K. Teo and N. Zheng, *J. Am. Chem. Soc.*, 2021, **143**, 10214-10220; (b) G. Deng, S. Malola, P. Yuan, X. Liu, B. K. Teo, H. Hakkinen and N. Zheng, *Angew. Chem. Int. Ed.*, 2021, **60**, 12897-12903.
16 Q. Sun, H.-H. Nie, H.-F. Su, S.-Y. Yang and B. K. Teo, *Inorg. Chem.*, 2020, **59**, 8836-8845.
17 A. K. Das, R. Mekkat, S. Maity, A. S. Nair, S. Bhandary, R. Bhowal, A. Patra, B. Pathak, D. Chopra and S. Mandal, *Inorg. Chem.*, 2021, **60**, 19270-19277.
18 Z. Wang, F.-L. Yang, Y. Yang, Q.-Y. Liu and D. Sun, *Chem. Commun.*, 2019, **55**, 10296-10299.
19 Z. Wang, Q.-P. Qu, H.-F. Su, P. Huang, R. K. Gupta, Q.-Y. Liu, C.-H. Tung, D. Sun and L.-S. Zheng, *Sci. China Chem.*, 2020, **63**, 16-20.
20 K. Yonesato, H. Ito, H. Itakura, D. Yokogawa, T. Kikuchi, N. Mizuno, K. Yamaguchi and K. Suzuki, *J. Am. Chem. Soc.*, 2019, **141**, 19550-19554.
21 X.-M. Luo, C.-H. Gong, X.-Y. Dong, L. Zhang and S.-Q. Zang, *Nano Res.*, 2021, **14**, 2309-2313.
22 Z. Wang, J.-W. Liu, H.-F. Su, Q.-Q. Zhao, M. Kurmoo, X.-P. Wang, C.-H. Tung, D. Sun and L.-S. Zheng, *J. Am. Chem. Soc.*, 2019, **141**, 17884-17890.
23 M.-Y. Gao, K. Wang, Y. Sun, D. Li, B.-Q. Song, Y. H. Andaloussi, M. J. Zaworotko, J. Zhang and L. Zhang, *J. Am. Chem. Soc.*, 2020, **142**, 12784-12790.
24 Z. Han, X.-Y. Dong, P. Luo, S. Li, Z.-Y. Wang, S.-Q. Zang and C. W. Mak Thomas, *Sci. Adv.*, 2020, **6**, eaay0107.